Engineering Reports

WILEY

Engineering Reports Open Access

RESEARCH ARTICLE OPEN ACCESS

Compartmental Modeling of Woodland Ecosystem Services for Evaluating Urban Natural Capital in Sustainable Cities

Kennedy Chinedu Okafor[1,2,3,4,5] | Kelvin Anoh[2] | Titus Ifeanyi Chinebu[5] | Omowunmi Mary Longe[3] | Simeon Keates[2]

[1]Imperial College London, South Kensington Campus, London, UK | [2]Center for Future Technologies, University of Chichester, Bognor Regis, UK | [3]Department of Electrical and Electronic Engineering Science, University of Johannesburg, Johannesburg, South Africa | [4]Smart Infrastructure and Industry Research (SIIR) Group, Department of Engineering, Manchester Metropolitan University, Manchester, UK | [5]Innovation Research Group, Federal University of Allied Health Sciences, Enugu, Nigeria

Correspondence: Kennedy Chinedu Okafor (kennedy.okafor@mmu.ac.uk)

Received: 16 March 2025 | **Revised:** 3 March 2026 | **Accepted:** 17 March 2026

Keywords: artificial intelligence | compartmental modeling | ecosystem services | non-standard finite difference | sustainable cities

ABSTRACT

Ecosystem services (ES) from natural assets such as woodlands, freshwater, and air are vital for human well-being and economic sustainability. In the UK, ES contribute approximately £1.5 trillion annually, with woodland ecosystem services (WES) alone valued at £382 billion. Key WES include carbon capture, air and water purification, recreation, and urban health services. Despite their significance, urban ES management often lacks comprehensive computational models for effective accounting and resource planning. When developed, sustainable smart city governance technologies such as the Internet of Things (IoT), artificial intelligence (AI), and predictive analytics can be integrated to enhance the forecasting and valuation of ES for natural capital accounting. In addition, other frameworks such as game theory, Leontief Input–Output analysis, gene–environment networks, and homogenization theory can be explored. This study models WES components as compartments using ordinary differential equations (ODEs) and incorporates management practices, such as forest conservation (e.g., reforestation), recreational infrastructure conservation (e.g., site hardening, visitor management), and water conservation (e.g., habitat protection, species management), as control variables. Since the resulting model is nonlinear and analytical solutions do not exist, we apply the widely used and complementary numerical methods, Non-Standard Finite Difference (NFSD) and Runge–Kutta 4th Order (RK4), to approximate solutions of such ODE problems, thereby preserving accuracy, stability, and nonnegativity. The NSFD and RK4 are applied to assess three critical WES: carbon sequestration, recreational infrastructure, and water filtration. The NSFD method is suited for global, long-term analyses and achieved up to 55.68% effectiveness, while RK4 is more appropriate for short-term, detailed dynamics and attained 48.66% effectiveness. These results highlight that compartmental modeling with either method can accurately capture ecosystem services for smart city planning and valuation. Both approaches are robust, with control variables such as reforestation enhancing carbon capture, improving water quality, and promoting urban health. This study emphasizes the importance of integrated governance frameworks that combine reforestation, conservation, and smart infrastructure policies to support long-term urban sustainability.

1 | Introduction

Although the study of ecosystem services has been around, the use of analytical modeling such as the compartmental modeling to understand ecosystem services for natural capital accounting, monitoring and management requires critical attention to support sustainable cities. A sustainable city prioritizes the well-being of its residents and the environment by minimizing its ecological footprint through reduced energy and resource consumption. It emphasizes sustainable urbanism, including efficient transportation, energy use, and waste management, resilience to climate change impacts, and the promotion of sustainable consumption and production patterns. Natural capital assets, such as woodland, offer a pathway to addressing critical societal challenges such as deteriorating recreational infrastructure, environmental degradation, housing shortages, water scarcity, and healthcare needs amid rapid population growth [1].

While numerous models of natural capital and ecosystem services exist [2–4], there are no comprehensive computational frameworks for natural capital accounting. Developing such models will enable governments to design evidence-based policies to replenish natural assets and ensure the sustainable use of existing resources across service domains in urban environments [1]. The use of computational modeling is crucial for stabilizing smart natural capital governance as it enables the simulation and analysis of complex environmental systems, allowing for the prediction of potential impacts and the optimisation of decision-making in real time. By incorporating advanced modeling tools, such as machine learning and AI, governance structures can assess interactions among various ecosystem services, identify risks, and forecast long-term changes across different policy scenarios. This enables more informed and precise resource management, ensuring that natural capital is preserved while addressing societal and economic needs. Computational models also enhance the ability to continuously monitor ecosystems, providing adaptive management strategies that respond to emerging challenges. This capability ensures the resilience and sustainability of natural resources. This study uses woodland ecosystem services (WES), a key natural capital asset, to present such a computational model.

Ecosystem services refer to the direct and indirect contributions of natural assets—such as woodland, ocean, freshwater, farmland, air, among others—to human well-being and quality of life [1]. WES are the benefits provided by woodlands to individuals and communities, particularly in urban environments. The UK woodland, for example, covers approximately 3.28 million hectares, representing 13% of the UK's land area in 2024, up from 7% in 1965. In 2021, its value was estimated at £382 billion [5]. UK woodlands provide four categories of ecosystem services: provisioning (e.g., fuel and fiber), regulating (e.g., climate, flood hazard, noise, and air quality regulation), cultural (e.g., cultural heritage, amenity, health, recreation, and tourism), and supporting (e.g., soil formation, often excluded from recent frameworks as an intermediate service) [6].

The UK Government, under the United Nations System of Environmental-Economic Accounting–Ecosystem Accounting (SEEA EA), is working to track changes in the extent and condition of ecosystems [5]. However, most existing models rely on time-series data from governmental agencies and lack comprehensive analytical approaches to describe ecosystem services in sustainable cities. Recent efforts, such as the European Commission's report in February 2023 [7], failed to comprehensively evaluate the roles of ecosystem services and their control variables. This study addresses these gaps by proposing a robust analytical model for ecosystem services, using woodland as a case study. The model offers insights into quantifying and optimizing the contributions of ecosystem services to human well-being, thereby supporting sustainable urban development. Although the study of ecosystem services and natural capital has been recognized globally since 1997 [8], the UK began exploring natural capital and the associated services and benefits to human well-being in December 2012. At that time, the Office for National Statistics (ONS) and the Department for Environment, Food and Rural Affairs (Defra) introduced work on how to account for the value that nature contributes to the UK's environmental accounts [9]. This value is referred to as the natural capital account.

Natural capital assets—such as woodlands, farmland, freshwater, and coastal areas—provide essential services, including energy, food, timber, air quality regulation, and recreation. These services, in turn, benefit human society. In the context of natural capital accounting, assets are considered "stocks," while the services they provide are referred to as "flows." Both stock and flow accounts can be represented in either monetary or physical terms [10, 11]. This study focuses on the flow of services that woodlands, as a form of natural capital, contribute to the UK's natural capital account. By quantifying woodland services, we aim to improve understanding and research into other natural capital stocks, facilitating more effective natural capital accounting. Ultimately, this approach will help achieve the United Nations Sustainable Development Goals (SDGs) and the UK's Net Zero targets.

In the UK, cities are increasingly relying on ecosystems and their services to support society and the economy [12]. These cities are being progressively developed into smart and sustainable urban environments. In 2007, Giffinger defined smart cities as "the search and identification of intelligent solutions which allow modern cities to enhance the quality of the services provided to citizens [13]." Based on their work, six key pillars of smart cities were identified: smart mobility, smart governance, smart economy, smart living, smart environment, and smart people [14]. Smart governance policies will drive the smart economy, smart living, smart environment, and smart mobility, while smart people will promote effective governance and sustainable cities, in line with the United Nations Sustainable Development Goals (SDGs). The United Nations Economic Commission for Europe (UNECE) describes "a smart sustainable city as an innovative city that uses Information and Communication Technologies (ICTs) and other means to improve quality of life, enhance the efficiency of urban operations and services, and boost competitiveness, all while meeting the needs of present and future generations across economic, social, environmental, and cultural dimensions" [15]. With the advent of the Internet of Things (IoT), data collection, machine learning and AI technologies, smart city governance, and modelling and accounting for WES based on analytical frameworks, natural capital accounting will become more attractive. For example, innovative frameworks such as game

theory, Leontief Input–Output analysis, gene–environment network and homogenization theory can be explored.

As the UK Government develops methods to track changes in ecosystem assets, computational modeling of WES offers a valuable empirical tool for studying, quantifying, and optimizing resource demand from natural assets while helping reduce emissions [11]. Such modeling offers smart, sustainable opportunities to integrate ecosystem services into natural capital accounting. In other words, ICTs, IoT, AI, sensors and other technologies can be leveraged to create resilient and efficient urban environments. There is a strong link between smart city governance and natural capital ecosystem services, as both are interconnected in fostering sustainable and liveable urban spaces. Ecosystem services, including air purification, water filtration, carbon sequestration, and biodiversity conservation, play a vital role in sustainability and resource management. The framework has been extended to an economy-wide material flow analysis (EW-MFA) [16]. In parallel, smart city governance leverages digital tools, IoT, and data-driven decision-making to optimize resource use and minimize environmental impacts. Urban planning and green infrastructure benefit significantly from natural capital assets, such as urban forests and wetlands, which contribute to improving air quality and help mitigate the urban heat island effect. For instance, governance frameworks increasingly incorporate geospatial mapping, AI, and analytics to embed ecosystem services into land-use strategies. These approaches form the foundation of an emerging smart city technology ecosystem that supports effective and sustainable governance [17].

Moreover, climate resilience is strengthened by integrating ecosystem service control variables within smart city systems. Predictive analytics and early warning systems enable cities to mitigate climate risks while aligning urban development with nature-based solutions. Citizen engagement further amplifies these efforts through participatory initiatives such as urban gardening and tree planting, which also raise public awareness about the importance of natural capital. In context, economic valuation and data-driven governance facilitate the integration of ecosystem services into policymaking, ensuring that urban growth aligns with long-term environmental sustainability [18]. The development of spatial data infrastructures (SDIs) underpins this process, improving local governance capacity and resilience.

Therefore, WES modeling serves as a powerful tool to quantify carbon sequestration, recreational infrastructure and water filtration and their benefits to human beings. Since this study views these components of WES as compartments, the inflow and outflow of resources over time will be described using ordinary differential equations (ODEs). It becomes essential to consider its stability properties, with linear stability often being a primary factor [19]. In cases where exact solutions to differential equations are unattainable, it becomes crucial to choose a numerical method that preserves the critical characteristics of the exact solution. Non-Standard Finite Difference (NSFD) methods and geometric numerical integrators play a vital role in ensuring that the numerical solution aligns with the essential properties of the system being modeled. Numerical solutions to differential equations are used to approximate their analytical counterparts, with methods such as NSFD and Runge–Kutta being commonly employed because they offer higher accuracy. For example, the Euler method, grounded in geometric intuition, approximates the solution by taking small steps [20]. It uses the slope at a given point to estimate the value of the solution at the next point. However, the Runge–Kutta method is a more sophisticated extension of the Euler method, offering higher accuracy. It improves on Euler's approach by incorporating multiple weighted slopes at each time step, enhancing the precision of the solution [21]. Among the various Runge–Kutta methods, the Runge–Kutta Fourth order (RK4) method is one of the oldest and most widely used techniques for solving ODEs. Its robustness and well-understood properties make it a popular choice for accurately solving a range of problems in numerical analysis. Following this present study, other methods such as game theory [22], Leontief Input–Output analysis [23–25], homogenization theory [26] and gene–environment network [27] can be studied.

The motivation for employing the NSFD and RK4 methods in modeling the integer-order derivatives of WES is to accurately capture the complex dynamics of these systems while ensuring precision, stability, and the preservation of key ecosystem properties. WES are intricate systems with interactions that can lead to non-negative populations, conservation of specific quantities, and possible oscillatory behavior. The NSFD method is particularly motivated by the need to maintain these properties in the discrete model. Unlike traditional methods, NSFD schemes can be customized to ensure that the numerical solution adheres to the computational constraints of the system, such as ensuring non-negativity of populations (e.g., tree densities, carbon stocks) over time. Given that WES often involve nonlinear interactions—such as carbon sequestration, water filtration, and recreational value—NSFD methods are designed to handle these nonlinearities while maintaining stability. This is a critical challenge with traditional methods, which often struggle with nonlinear differential equations.

Although RK4 is not specifically designed for nonlinear systems, it remains highly effective for many practical problems, including those with moderate nonlinearity, because of its high accuracy and ease of implementation. In modeling ecosystem services, accurately examining the long-term behavior of the system is crucial. This includes maintaining key quantities, such as total biomass or energy, and ensuring correct asymptotic behavior. While NSFD methods are specifically built to respect these conservation laws and asymptotic properties, RK4, although not inherently focused on conservation, can still serve as a useful baseline for comparison. It can be effectively combined with conservation-focused methods like NSFD to improve the modeling process.

The main contributions of this study are:

- Formulating WES into an analytical model with control variables to assess ecosystem stock and flow dynamics, supporting natural capital accounting in sustainable city economies. Three examples of WES (e.g., carbon sequestration, recreation and water filtration) are used, while three management

practices (e.g., reforestation, recreational infrastructure conservation and water conservation) were introduced as the control variables.

- Applying conservation-focused numerical tools for short-term precision (e.g., RK4) and long-term stability (e.g., NSFD), ensuring accurate and stable results essential for sustainable ecosystem governance.
- Analyzing resource management impact using the proposed model and evaluating management practices (e.g., reforestation, recreational infrastructure conservation and water conservation). Results show that balanced resource allocation is key to preventing ecosystem strain.
- Demonstrating adaptive policy management as a mechanism to balance interventions in critical areas, allowing policymakers to adjust strategies for ecosystem resilience and urban sustainability

The remaining parts of the article are organized as follows: Section 2 introduces the formulation of the integer-order derivative model. Section 3 details the numerical modeling. Section 4 presents the numerical simulation results and discussion. Finally, Section 5 concludes the work.

2 | Problem Formulation and WES Model

This section explains the integer-order derivative model in a simple form. Consider a woodland ecosystem that delivers multiple ecosystem services, as illustrated in Figure 1a. These services include biodiversity conservation, carbon sequestration (greenhouse gas regulation), recreation and tourism, and water filtration. The WES model is developed to investigate the performance of ecosystem stocks and flows within an economy. The model is formulated as an integer-order dynamic system, which captures the time-evolving nature of these processes. We approach the problem as a dynamic system, consisting of equations that describe the natural processes governing the ecosystem. These processes evolve over time and are central to understanding the interaction between ecosystem services and their impact on environmental and economic systems [29].

Using the parameter descriptions in Table 1 and the transfer diagram in Figure 1b, this study presents the WES model as a system of integer derivatives, governed by three primary variables:

- Biodiversity and Carbon Sequestration, that is, (Greenhouse gas regulation) $X(t)$, sourced from remote sensing and carbon flux measurements, governed by intergovernmental

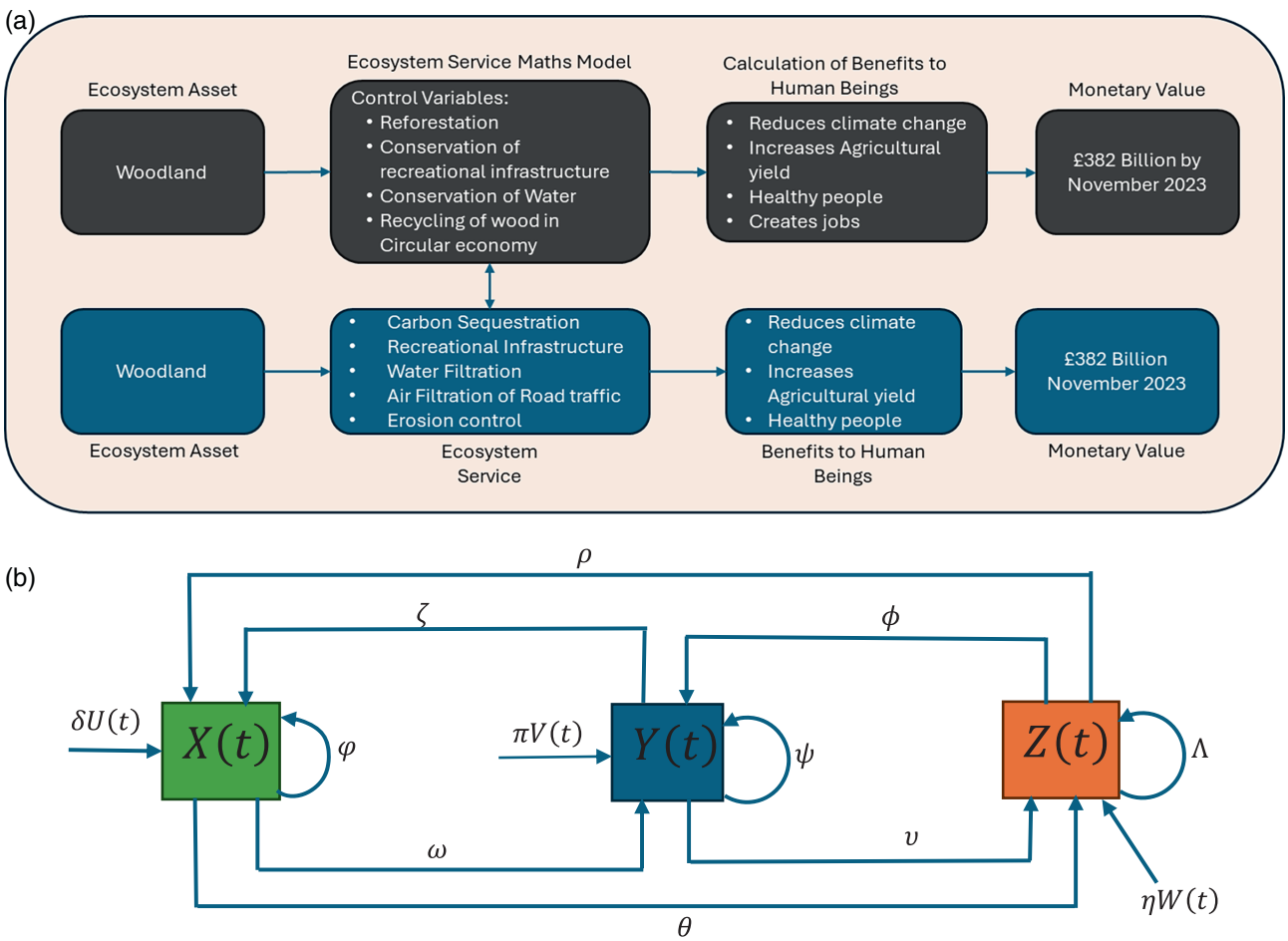

FIGURE 1 | (a) Proposed engineering data governance model for ecosystem services within the context of natural capital and sustainable cities, using woodland as a case study. This model is inspired by the generalized natural capital logic chain outlined by Natural England [28], supported by insights from the Office for National Statistics report and aligned with the defining characteristics established by the UK Government [5]. (b) Natural Capital Asset Framework of the compartmental flow of resources in woodland ecosystem services.

TABLE 1 | Parameters and constants for woodland ecosystem model.

Parameter	Description
φ	The rate at which carbon stock increases or decreases naturally, without any external influence.
δ	Effectiveness of reforestation efforts $U(t)$ on increasing carbon stock.
ζ	Influence of climate change on carbon stock.
ρ	Impact of water quality Z on carbon sequestration $X(t)$
ψ	Self-regulation coefficient for recreational value $Y(t)$. It represents the natural rate of change in recreational value, considering factors like ecosystem attractiveness, biodiversity, and user experience. A positive value indicates an increase in recreational value over time, while a negative value indicates a decrease.
π	Control coefficient for recreational infrastructure development $V(t)$ on recreational value $Y(t)$. It represents the impact of investing in recreational infrastructure (like trails, facilities, or educational programs) on enhancing the recreational experience and value.
ω	Interaction coefficient representing the effect of water quality $Z(t)$ on recreational value $Y(t)$. A positive value indicates improved water quality enhances recreational value (e.g., clearer water attracts more users), while a negative value indicates a negative impact (e.g., poor water quality deters users).
ϕ	External influence coefficient representing the impact of external factors on recreational value $Y(t)$.
Λ	Self-regulation coefficient for water quality $Z(t)$. It represents the natural rate of change in water quality, considering factors like water cycles, natural filtration, and ecosystem balance. A positive value indicates improvement in water quality over time, while a negative value indicates degradation.
η	Control coefficient for water conservation efforts $W(t)$ on water quality $Z(t)$. It represents the effectiveness of water conservation measures (like reducing pollution or implementing efficient water use practices) in improving water quality.
θ	Interaction coefficient representing the effect of carbon stock $X(t)$ on water quality $Z(t)$. A positive value indicates that increased carbon stock improves water quality (e.g., through natural filtration), while a negative value indicates a negative impact (e.g., increased runoff).
υ	External influence coefficient representing the impact of external factors (like climate change, population growth, or policy changes) on water quality $Z(t)$.
γ	Forest management intensity (e.g., reforestation rate)
K_1	Carrying capacity of the forest ecosystem
K_2	Threshold value for recreational activities
α_1	Exponent representing the nonlinear effect of recreational activities on forest management
ε	Recreational infrastructure development rate
K_4	Carrying capacity of recreational activities
K_3	Threshold value for forest ecosystem health
α_2	Exponent showing the nonlinear effect of forest ecosystem health on recreational infrastructure development
α_3	Exponents representing the nonlinear effects of forest ecosystem health on conservation efforts
α_4	Exponents showing the nonlinear effects of forest ecosystem recreational activities on conservation efforts
σ	Conservation effort intensity
K_5	Carrying capacity of water filtration

panel on climate change (IPCC) compliance, AI-driven validation, and open climate research access;

- Recreation and Tourism $Y(t)$, derived from visitor surveys and geospatial tracking, ensuring general data protection regulation (GDPR) compliance, data-sharing agreements, and economic integration.
- Water Filtration $Z(t)$, monitored via hydrological models and IoT sensors, adhering to national water quality standards and restricted access policies.

The transfer diagram in Figure 1b illustrates the interdependencies among these variables, where changes in one factor influence the others, reinforcing the need for robust governance mechanisms to ensure data integrity, interoperability, and secure access within the Natural Capital Asset Framework (NCAF).

The model parameters are outlined in Table 1. These constants represent the complex relationships among ecosystem services, their impacts on management practices, interactions, and external factors. By estimating these parameters, we can gain a deeper understanding of how the woodland ecosystem responds to various scenarios, thereby facilitating more informed and effective decision-making.

From the compartmental model in Figure 1b, the ecosystem services (i.e., flows—both inflow (+) and outflow (−) of resources)

derived from woodland as a natural capital asset (or stock) can be expressed as follows:

$$\frac{dX}{dt} = \varphi X(t) + \delta U(t) + \zeta Y(t) + \rho Z(t) - (\omega + \theta)X(t), \tag{1a}$$

$$\frac{dY}{dt} = \psi Y(t) + \pi V(t) + \omega X(t) + \phi Z(t) - (\zeta + \upsilon)Y(t), \tag{1b}$$

$$\frac{dZ}{dt} = \Lambda Z(t) + \eta W(t) + \theta X(t) + \upsilon Y(t) - (\rho + \phi)Z(t). \tag{1c}$$

Let the initial boundary conditions be $X(0) \geq 0, Y(0) \geq 0$ and $Z(0) \geq 0$. From the model Equations (1a–c), forest management practices (e.g., reforestation, thinning) $U(t)$, recreational infrastructure conservation $V(t)$ and water conservation efforts (e.g., habitat protection, species management) $W(t)$represent the control variables when evaluating the performance of ecosystem stock and flow in an economy. Here, we can define:

$$U(t) = \gamma\left(1 - \frac{X}{K_1}\right)\left(\frac{Y}{K_2}\right)^{\alpha_1}, \tag{2a}$$

$$V(t) = \varepsilon\left(1 - \frac{Y}{K_4}\right)\left(\frac{X}{K_3}\right)^{\alpha_2}, \tag{2b}$$

$$W(t) = \sigma\left(1 - \frac{Z}{K_5}\right)\left(\frac{X}{K_3}\right)^{\alpha_3}\left(\frac{Y}{K_2}\right)^{\alpha_4}. \tag{2c}$$

By substituting Equations (2a–c) into Equations (1a–c), the WES model in terms of the control variables can be rewritten as:

$$\frac{dX}{dt} = \varphi X(t) + \delta\gamma\left(1 - \frac{X(t)}{K_1}\right)\left(\frac{Y(t)}{K_2}\right)^{\alpha_1} + \zeta Y(t) + \rho Z(t) - (\omega + \theta)X(t), \tag{3a}$$

$$\frac{dY}{dt} = \psi Y(t) + \pi\varepsilon\left(1 - \frac{Y(t)}{K_4}\right)\left(\frac{X(t)}{K_3}\right)^{\alpha_2} + \omega X(t) + \phi Z(t) - (\zeta + \upsilon)Y(t), \tag{3b}$$

$$\frac{dZ}{dt} = \Lambda Z(t) + \eta\sigma\left(1 - \frac{Z(t)}{K_5}\right)\left(\frac{X(t)}{K_3}\right)^{\alpha_3}\left(\frac{Y(t)}{K_2}\right)^{\alpha_4} + \theta X(t) + \upsilon Y(t) - (\rho + \phi)Z(t). \tag{3c}$$

The control variables $U(t)$, $V(t)$ and $W(t)$ represent the management and conservation practices that impact the ecosystem services. Clearly, as the control variables of the ecosystem services model in Equations (2a–c) are nonlinear, the linear WES model in Equations (1a–c), as an integer-order model, becomes nonlinear in Equations (3a–c).

The compartmental model developed in Equations (3a–c) can be applied to explore several other aspects of ecosystem services. For instance, Equations (3a–c) can help deepen understanding of the link between ecosystem services and human well-being concerning recreational infrastructure, such as parks, play centres, and exercise facilities. The model in Equations (3a–c) can also be used to assess intervention parameters that influence the relationship between ecosystem services and the well-being of rural residents in a specific community. Likewise, the model can predict biodiversity levels and the success of climate change interventions in river basins, tropical regions, towns, and cities. Additionally, the compartmental model in Equations (3a–c) can offer insights into the roles of control variables on carbon capture, air and water quality, recreational infrastructure, and the health status of a particular geographical area. Based on these broad areas of potential applications of the model, electronic sensors, geospatial information systems (GIS), and the data generated from them can be approached using machine learning integrated into the study of ecosystem services.

2.1 | Non-Negativity and Boundedness of Solution

Since the study concerns natural resources, all components of the solution to the differential equations must be non-negative (i.e., positive or zero values). Similarly, because natural resources are quantifiable and finite, the solution must remain within a finite range rather than grow without bound. To analyze the non-negativity and boundedness of the solution for the system of differential equations provided, we need to demonstrate that the solution $X(t), Y(t)$, and $Z(t)$, remain non-negative and bounded for all $t \geq 0$, provided the initial conditions $X(0), Y(0)$, and $Z(0)$ are non-negative, and certain conditions hold for the parameters and control functions $U(t), V(t)$, and $W(t)$. From Equations (3a–c) we can discuss the non-negativity, boundedness and existence and uniqueness analyses.

2.1.1 | Non-Negativity Analysis

In this model, $U(t)$, $Y(t)$, and $Z(t)$ represent control-related variables corresponding respectively to *reforestation or forest management efforts*, *recreational activity intensity*, and *water filtration or conservation practices*. Each of these control variables is defined within a biologically admissible set such that $U(t), Y(t), Z(t) \geq 0$ for all $t \geq 0$, since negative values (e.g., "negative reforestation effort" or "negative water conservation") are not meaningful in ecological or policy terms. The coefficients δ, ζ, and ρ are positive parameters quantifying the effects of these controls on carbon sequestration dynamics and therefore, under the ecological and control admissibility assumptions $U(t), Y(t), Z(t) \geq 0$ and $\delta, \zeta, \rho > 0$, the products $\delta U(t), \zeta Y(t), \rho Z(t)$ are non-negative.

Thus, to prove the non-negativity of the solutions $X(t), Y(t)$ and $Z(t)$, show that if $X(0) \geq 0, Y(0) \geq 0$ and $Z(0) \geq 0$, then $X(t) \geq 0, Y(t) \geq 0$ and $Z(t) \geq 0$ for all $t \geq 0$. Then, from Equation (1a) we have

$$\begin{aligned}\frac{dX}{dt} &= \varphi X(t) + \delta U(t) + \zeta Y(t) + \rho Z(t) - (\omega + \theta)X(t),\\ &\geq -(\omega + \theta)X(t).\end{aligned} \tag{4a}$$

Solving (4b) gives

$$X(t) \geq X(0)\exp(-(\omega + \theta))t \geq 0. \tag{4b}$$

This implies that $X(t) > 0$, for all $t \geq 0$. The terms $\delta U(t), \zeta Y(t)$ and $\rho Z(t)$ are non-negative, ensuring that the positive contributions to $\frac{dX}{dt}$ will always be greater than or equal to the negative term $(\omega + \theta)X(t)$. Therefore, if $X(0) \geq 0$, then $X(t) \geq 0$, for all $t \geq 0$. Similarly, from Equation (1b), we obtain

$$\begin{aligned}\frac{dY}{dt} &= \psi Y(t) + \pi V(t) + \omega X(t) + \phi Z(t) - (\zeta + \upsilon)Y(t),\\ &\geq -(\zeta + \upsilon)Y(t).\end{aligned} \tag{5a}$$

If $Y(0) \geq 0$ and given that $\pi V(t), \omega X(t)$ and $\phi Z(t)$, are non-negative, the equation ensures that $Y(t) > 0 \forall\, t \geq 0$, thus:

$$Y(t) \geq Y(0)\exp(-(\zeta + \upsilon))t \geq 0. \tag{5b}$$

Finally, from Equation (1c), we get

$$\begin{aligned}\frac{dZ}{dt} &= \Lambda Z(t) + \eta W(t) + \theta X(t) + \upsilon Y(t) - (\rho + \phi)Z(t),\\ &\geq -(\rho + \phi)Z(t)\end{aligned} \tag{6a}$$

Similarly, $Z(t) > 0$ for all $t \geq 0$, provided that $Z(0) > 0$, thus we obtain;

$$Z(t) \geq Z(0)\exp(-(\rho + \phi))\, t \geq 0. \tag{6b}$$

2.1.2 | Boundedness Analysis

For boundedness, we need to show that $X(t)$, $Y(t)$, and $Z(t)$ do not grow indefinitely as t increases. Therefore, let $U(t), V(t)$,and $W(t)$ be bounded functions, and let $X(t), Y(t)$, and $Z(t)$ be non-negative. The growth of $X(t)$ is limited by the negative term $(\omega + \theta)X(t)$. Therefore, $X(t)$ is bounded if the sum of the non-negative terms does not exceed the natural decay rate $(\omega + \theta)X(t)$.

Similarly, for , $Y(t)$ and $Z(t)$, the presence of the negative terms $(\zeta + \upsilon)Y(t)$ and $(\rho + \phi)Z(t)$ will limit the growth of $Y(t)$ and $Z(t)$, respectively, ensuring that both remain bounded. Given the non-negative initial conditions $X(0) \geq 0, Y(0) \geq 0$ and $Z(0) \geq 0$ the solutions $X(t), Y(t)$, and $Z(t)$ of the system are non-negative and bounded for non-negative initial conditions and bounded control inputs. This ensures that the solutions are physically meaningful in the context of WES.

2.1.3 | Existence and Uniqueness of the Model

To demonstrate the existence and uniqueness of the solution for the system of differential equations in the WES model, we typically rely on the Picard-Lindelöf theorem (also known as the Cauchy-Lipschitz theorem) for ordinary differential equations (ODEs). This theorem asserts that a system of differential equations will have a unique solution if the following conditions are satisfied:

- Continuity: The function defining the system must be continuous with respect to its variables and parameters. (The right-hand side (RHS) of the differential equations should be continuous);
- Lipschitz Condition: The function defining the system must satisfy a Lipschitz condition in the dependent variable, ensuring that changes in the solution are proportional to changes in the initial conditions. That is, the RHS of the differential equations should satisfy a Lipschitz condition with respect to the dependent variables.

These conditions guarantee that for any given initial condition, a unique solution exists to the system of differential equations in a neighbourhood around the initial condition.

Considering Equations (4a), (5a) and (6a), we rewrite the system of equations in the standard form for ODEs:

$$\frac{dQ}{dt} = F(t, Q). \tag{7}$$

where $Q(t) = [X(t)\, Y(t)\, Z(t)]^T$. The function $F(t, Q)$ is a linear combination of the variables $X(t), Y(t)$ and $Z(t)$, with coefficients that are continuous functions of time t. Therefore, $F(t, Q)$ is continuous with respect to both t and Q. To satisfy the Lipschitz condition, we check whether there exists a constant $L >$ 0such that:

$$\left\| F(t, Q_1) - F(t, Q_2) \right\| \leq L \| Q_1 - Q_2 \|. \tag{8}$$

for any two vectors $Q_1, Q_2 \in R^3$. Given the linear nature of $F(t, Q)$, the difference $F(t, Q_1) - F(t, Q_2)$ will yield a linear expression in the differences $X_1 - X_2, Y_1 - Y_2$ and $Z_1 - Z_2$. Therefore, a Lipschitz constant L can be determined from the maximum of the absolute values of the coefficients φ, $\delta, \zeta, \rho, \omega, \theta, \psi, \pi, \phi, \zeta, \upsilon, \Lambda, \eta$ (and potentially other coefficients involved), ensuring that the Lipschitz condition is satisfied. Since, $F(t, Q)$ is continuous and satisfies the Lipschitz condition, the system of differential equations has a unique solution that exists on some interval containing the initial time t_0, according to the Picard-Lindelöf theorem. This confirms the existence and uniqueness of the solution for the given system of equations under the stated assumptions. Since smart city governance with emerging technologies could provide solid implementation framework to optimize the management and integration of ecosystem services within urban environments, in Section 2, we shall introduce two finite difference (FD) methods to solve the system model in Equations (1a–c).

We now extended the existence/uniqueness discussion to address the more complex, nonlinear form of the final model with control variables substituted (Equations 3a–c), which is the model actually simulated. Write the right-hand side vector field as $F(X, Y, Z) = \left(F_1, F_2, F_3\right)^{\top}$. Let the Jacobian $J(X, Y, Z) = \left(\frac{\partial F_i}{\partial \rho}\right)$ and computing the partial derivatives symbolically we have

$$J(X, Y, Z) = \begin{bmatrix} \frac{\partial F_1}{\partial X} & \frac{\partial F_1}{\partial Y} & \frac{\partial F_1}{\partial Z} \\ \frac{\partial F_2}{\partial X} & \frac{\partial F_2}{\partial Y} & \frac{\partial F_2}{\partial Z} \\ \frac{\partial F_3}{\partial X} & \frac{\partial F_3}{\partial Y} & \frac{\partial F_3}{\partial Z} \end{bmatrix}$$

where

$$\frac{\partial F_1}{\partial X} = \phi - \delta\gamma \frac{1}{K_1}\left(\frac{Y}{K_2}\right)^{\alpha_1} - (\omega + \theta),$$

$$\frac{\partial F_1}{\partial Y} = \delta\gamma\left(1 - \frac{X}{K_1}\right)\alpha_1\left(\frac{Y}{K_2}\right)^{\alpha_1 - 1}\frac{1}{K_2} + \zeta,$$

$$\frac{\partial F_1}{\partial Z} = \rho,$$

$$\frac{\partial F_2}{\partial X} = \pi\varepsilon\left(1 - \frac{Y}{K_4}\right)\alpha_2\left(\frac{X}{K_3}\right)^{\alpha_2 - 1}\frac{1}{K_3} + \omega,$$

$$\frac{\partial F_2}{\partial Y} = \psi - \pi\varepsilon\frac{1}{K_4}\left(\frac{X}{K_3}\right)^{\alpha_2} - (\zeta + \upsilon),$$

$$\frac{\partial F_2}{\partial Z} = \varphi,$$

$$\frac{\partial F_3}{\partial X} = \eta\sigma\left(1 - \frac{Z}{K_5}\right)\alpha_3\left(\frac{X}{K_3}\right)^{\alpha_3 - 1}\frac{1}{K_3}\left(\frac{Y}{K_2}\right)^{\alpha_4} + \theta,$$

$$\frac{\partial F_3}{\partial Y} = \eta\sigma\left(1-\frac{Z}{K_5}\right)\left(\frac{X}{K_3}\right)^{\alpha_3}\alpha_4\left(\frac{Y}{K_2}\right)^{\alpha_4-1}\frac{1}{K_2}+\upsilon,$$

$$\frac{\partial F_3}{\partial Z} = \Lambda-\eta\sigma\frac{1}{K_5}\left(\frac{X}{K_3}\right)^{\alpha_3}\left(\frac{Y}{K_2}\right)^{\alpha_4}-(\rho+\varphi).$$

All entries are elementary algebraic expressions of X, Y, Z and the (positive) parameters. For continuity and boundedness of Jacobian on a biologically admissible compact set, we let the biologically admissible compact domain be

$$\mathcal{D} = \{(X,Y,Z) : 0 \le X \le \overline{X}, 0 \le Y \le \overline{Y}, 0 \le Z \le \overline{Z}\},$$

where a natural choice is $\overline{X} = K_1, \overline{Y} = K_2, \overline{Z} = K_5$ On $\mathcal{D}$:

- Every entry of the Jacobian is continuous (composition of continuous functions) whenever the power functions $(\cdot)^{\alpha_i-1}$are well defined and finite on $\mathcal{D}$.
- If each exponent satisfies $\alpha_i \ge 1$(so the derivatives $\alpha(X)^{\alpha_i-1}$or $(Y)^{\alpha_i-1}$ remain bounded on $\mathcal{D}$, including at zero), then each partial derivative is bounded on $\mathcal{D}$. Hence, the Jacobian is bounded and continuous on the compact set $\mathcal{D}$. By standard results, a bounded continuous Jacobian $\Rightarrow$ $F$is Lipschitz on $\mathcal{D}$. Therefore, a global Lipschitz constant L exists:

$$L = \underset{(X,Y,Z)\in D}{\text{maximise}} \sum_{j=1}^{3}\left|\frac{\partial F_i}{\partial \wp}\right| \qquad (\wp = X, Y, Z \text{ and } i = 1,2,3).$$

Under the biologically admissible compact set $\mathcal{D}$ and the assumption that $\alpha_i \ge 1$for all i, state variables remain bounded away from zero, the Jacobian is continuous and bounded on $\mathcal{D}$, hence $F$is Lipschitz on $\mathcal{D}$. Therefore, for initial data in $\mathcal{D}$, the nonlinear system (Equations 3a–c) admits a unique solution.

3 | Numerical Modeling

In this subsection, the RK4 and NSFD schemes are employed to computationally fix model Equations (1a–c). In Section 4, we will compare the results obtained from the NSFD method with those derived from the standard RK4 method, using the MATLAB computational engine.

3.1 | Runge–Kutta Method of Order 4

Here, we shall develop the RK4-FD scheme for model Equations (1a–c), thus:

$$X_{n+1}-X_n = h\left[\varphi X_n+\delta\gamma\left(1-\frac{X_n}{K_1}\right)\left(\frac{Y_n}{K_2}\right)^{\alpha_1}+\zeta Y_n+\rho Z_n-(\omega+\theta)X_n\right], \tag{9a}$$

$$Y_{n+1}-Y_n = h\left[\psi Y_n+\pi\varepsilon\left(1-\frac{Y_n}{K_4}\right)\left(\frac{X_n}{K_3}\right)^{\alpha_2}+\omega X_n+\phi Z_n-(\zeta+\upsilon)Y_n\right], \tag{9b}$$

$$Z_{n+1}-Z_n = h\left[\Lambda Z_n+\eta\sigma\left(1-\frac{Z_n}{K_5}\right)\left(\frac{X_n}{K_3}\right)^{\alpha_3}\left(\frac{Y_n}{K_2}\right)^{\alpha_4}+\theta X_n+\upsilon Y_n-(\rho+\phi)Z_n\right]. \tag{9c}$$

Equations (9a–c) can be rewritten as:

$$X_{n+1} = X_n+h\left[\varphi X_n+\delta\gamma\left(1-\frac{X_n}{K_1}\right)\left(\frac{Y_n}{K_2}\right)^{\alpha_1}+\zeta Y_n+\rho Z_n-(\omega+\theta)X_n\right], \tag{10a}$$

$$Y_{n+1} = Y_n+h\left[\psi Y_n+\pi\varepsilon\left(1-\frac{Y_n}{K_4}\right)\left(\frac{X_n}{K_3}\right)^{\alpha_2}+\omega X_n+\phi Z_n-(\zeta+\upsilon)Y_n\right], \tag{10b}$$

$$Z_{n+1} = Z_n+h\left[\Lambda Z_n+\eta\sigma\left(1-\frac{Z_n}{K_5}\right)\left(\frac{X_n}{K_3}\right)^{\alpha_3}\left(\frac{Y_n}{K_2}\right)^{\alpha_4}+\theta X_n+\upsilon Y_n-(\rho+\phi)Z_n\right]. \tag{10c}$$

Finding X_{n+1}, Y_{n+1} and Z_{n+1} requires four intermediate calculations as shown in Section A.1 of the Appendix A.

3.2 | Non-Standard Finite Difference Scheme (NSFD)

We design the NSFD scheme to replicate the dynamics of the continuous model system Equations (1a–c). The NSFD scheme, introduced by Mickens in 1989 [30], has since become widely adopted for solving systems of differential equations in fields such as mathematical biology and other related disciplines [31]. This method has proven superior in preserving passivity [32, 33], compared to other well-known numerical methods for state-variable systems. The NSFD scheme ensures dynamic consistency and numerical stability, even when using irregular step lengths. The formulation of model Equations (1a–c) is based on the principles established by Mickens.

$$\frac{X_{n+1}-X_n}{h} = \varphi X_{n+1}+\delta\gamma\left(1-\frac{X_{n+1}}{K_1}\right)\left(\frac{Y_n}{K_2}\right)^{\alpha_1}+\zeta Y_n+\rho Z_n-(\omega+\theta)X_{n+1}, \tag{11a}$$

$$\frac{Y_{n+1}-Y_n}{h} = \psi Y_{n+1}+\pi\varepsilon\left(1-\frac{Y_{n+1}}{K_4}\right)\left(\frac{X_n}{K_3}\right)^{\alpha_2}+\omega X_n+\phi Z_n-(\zeta+\upsilon)Y_{n+1}, \tag{11b}$$

$$\frac{Z_{n+1}-Z_n}{h} = \Lambda Z_{n+1}+\eta\sigma\left(1-\frac{Z_{n+1}}{K_5}\right)\left(\frac{X_n}{K_3}\right)^{\alpha_3}\left(\frac{Y_n}{K_2}\right)^{\alpha_4}+\theta X_n+\upsilon Y_n-(\rho+\phi)Z_{n+1}. \tag{11c}$$

These NSFD equations of the WES can be rewritten as:

$$X_{n+1} = \frac{X_n+h\delta\gamma\left(\frac{Y_n}{K_2}\right)^{\alpha_1}+h\zeta Y_n+h\rho Z_n}{1+h\delta\gamma\left(\frac{1}{K_1}\right)\left(\frac{Y_n}{K_2}\right)^{\alpha_1}+h(\omega+\theta)-h\varphi}, \tag{12a}$$

$$Y_{n+1} = \frac{Y_n+h\pi\varepsilon\left(\frac{X_n}{K_3}\right)^{\alpha_2}+h\omega X_n+h\phi Z_n}{1+h\pi\varepsilon\left(\frac{1}{K_4}\right)\left(\frac{X_n}{K_3}\right)^{\alpha_2}+h(\zeta+\upsilon)-h\psi}, \tag{12b}$$

$$Z_{n+1} = \frac{Z_n+h\eta\sigma\left(\frac{X_n}{K_3}\right)^{\alpha_3}\left(\frac{Y_n}{K_2}\right)^{\alpha_4}+h\theta X_n+h\upsilon Y_n}{1+h\eta\sigma\left(\frac{1}{K_5}\right)\left(\frac{X_n}{K_3}\right)^{\alpha_3}\left(\frac{Y_n}{K_2}\right)^{\alpha_4}+h(\rho+\phi)-h\Lambda}. \tag{12c}$$

To obtain success in NSFD, Equations (12a–c) should be sequentially computed since the value of X_{n+1} will be applied in calculating Y_{n+1} which in turn is then used in computing Z_{n+1}. The process is repeated until we finally approach the time of interest.

3.3 | Convergence Analysis of the NSFD Scheme

The NSFD scheme converges to the equilibrium point when the absolute value of the eigenvalues is less than one. In this subsection, we will examine the convergence of the proposed NSFD scheme using the following methods:

$$A = \frac{X + h\delta\gamma\left(\frac{Y}{K_2}\right)^{\alpha_1} + h\zeta Y + h\rho Z}{1 + h\delta\gamma\left(\frac{1}{K_1}\right)\left(\frac{Y}{K_2}\right)^{\alpha_1} + h(\omega+\theta) - h\varphi}, \tag{13a}$$

$$B = \frac{Y + h\pi\varepsilon\left(\frac{X}{K_3}\right)^{\alpha_2} + h\omega X + h\phi Z}{1 + h\pi\varepsilon\left(\frac{1}{K_4}\right)\left(\frac{X}{K_3}\right)^{\alpha_2} + h(\zeta+\upsilon) - h\psi}, \tag{13b}$$

$$C = \frac{Z + h\eta\sigma\left(\frac{X}{K_3}\right)^{\alpha_3}\left(\frac{Y}{K_2}\right)^{\alpha_4} + h\theta X + h\upsilon Y}{1 + h\eta\sigma\left(\frac{1}{K_5}\right)\left(\frac{X}{K_3}\right)^{\alpha_3}\left(\frac{Y}{K_2}\right)^{\alpha_4} + h(\rho+\phi) - h\Lambda}. \tag{13c}$$

For simplification, we let $\alpha_1 = \alpha_2 = \alpha_3 = \alpha_4 = 1$, and then obtain the following:

$$A = \frac{X + h\delta\gamma\left(\frac{Y}{K_2}\right) + h\zeta Y + h\rho Z}{1 + h\delta\gamma\left(\frac{1}{K_1}\right)\left(\frac{Y}{K_2}\right) + h(\omega+\theta) - h\varphi}, \tag{14a}$$

$$B = \frac{Y + h\pi\varepsilon\left(\frac{X}{K_3}\right) + h\omega X + h\phi Z}{1 + h\pi\varepsilon\left(\frac{1}{K_4}\right)\left(\frac{X}{K_3}\right) + h(\zeta+\upsilon) - h\psi}, \tag{14b}$$

$$C = \frac{Z + h\eta\sigma\left(\frac{X}{K_3}\right)\left(\frac{Y}{K_2}\right) + h\theta X + h\upsilon Y}{1 + h\eta\sigma\left(\frac{1}{K_5}\right)\left(\frac{X}{K_3}\right)\left(\frac{Y}{K_2}\right) + h(\rho+\phi) - h\Lambda}. \tag{14c}$$

The partial derivatives of A, B and C with respect to X, Y and Z, respectively, are shown in Appendix A.5.

3.4 | Stability Analysis of the Model

For the stability analysis of the given system of equations, we will focus on the equilibrium points and determine the conditions under which the system remains stable. This involves examining the eigenvalues of the Jacobian matrix of Equations (1a–c) at the equilibrium points and assessing whether their absolute values are less than one, indicating stability.

To find the equilibrium points, we set $\frac{dX}{dt} = \frac{dY}{dt} = \frac{dZ}{dt} = 0$. Solving the system for X^*, Y^*, Z^* An equilibrium (X^*, Y^*, Z^*) satisfies:

$$X_{n+1} = X_n = X^*, Y_{n+1} = Y_n = Y^*, Z_{n+1} = Z_n = Z^* \tag{15}$$

Linearise the system around the equilibrium point (X^*, Y^*, Z^*). The linearised system can be represented as:

$$\frac{d}{dt}\begin{pmatrix}\Delta X\\ \Delta Y\\ \Delta Z\end{pmatrix} = J\begin{pmatrix}\Delta X\\ \Delta Y\\ \Delta Z\end{pmatrix}, \tag{16}$$

subject to $J(\cdot)$, the Jacobian matrix evaluated at the equilibrium point (X^*, Y^*, Z^*) which can be rewritten as:

$$J\begin{pmatrix}\Delta X\\ \Delta Y\\ \Delta Z\end{pmatrix} = \begin{bmatrix}\frac{\partial A}{\partial X} & \frac{\partial A}{\partial Y} & \frac{\partial A}{\partial Z}\\ \frac{\partial B}{\partial X} & \frac{\partial B}{\partial Y} & \frac{\partial B}{\partial Z}\\ \frac{\partial C}{\partial X} & \frac{\partial C}{\partial Y} & \frac{\partial C}{\partial Z}\end{bmatrix} = \begin{bmatrix}A_{11} & A_{12} & A_{13}\\ B_{21} & B_{22} & B_{23}\\ C_{31} & C_{32} & C_{33}\end{bmatrix}, \tag{17}$$

subject to A, B and C, the right-hand sides of Equations (1a–c) and the matrix elements are determined as shown in Section 5.

3.5 | Eigenvalue Analysis

The eigenvalues of the Jacobian matrix, J, are used to determine the stability of the equilibrium point. The characteristic equation for the eigenvalues $\lambda$of the Jacobian matrix J is given by:

$$|\, J - \lambda \mathbf{I} \,| = 0, \tag{18}$$

subject to $\mathbf{I}$, the identity matrix. From the determinant of model in (1), the characteristic equation can be found as:

$$\begin{vmatrix}(A_{11}-\lambda) & A_{12} & A_{13}\\ B_{21} & (B_{22}-\lambda) & B_{23}\\ C_{31} & C_{32} & (C_{33}-\lambda)\end{vmatrix} = 0, \tag{19a}$$

$$\begin{aligned}&\lambda^3 - (A_{11}+B_{22}+C_{33})\lambda^2\\ &+ (A_{11}B_{22} + A_{11}C_{33} + B_{22}C_{33} - A_{12}B_{21} - A_{13}C_{31} - B_{23}C_{32})\lambda\\ &+ A_{11}B_{23}C_{32} + A_{12}B_{21}C_{33} + A_{13}B_{22}C_{31} - A_{12}B_{23}C_{31}\\ &- A_{11}B_{22}C_{33} - A_{13}B_{21}C_{32} = 0.\end{aligned} \tag{19b}$$

To find the eigenvalues of a third-degree polynomial used in a finite difference scheme's stability analysis, we form the characteristic equation of the system's matrix, then solve this cubic polynomial for its roots, which are the eigenvalues. For complex cubic polynomials, the most practical method is to use a numerical solver in software like MATLAB. For stability, all eigenvalues must satisfy the condition that their magnitude is less than or equal to 1 (or some other threshold depending on the scheme and norms used). The spectral radius $\mathscr{R}(J)$ is the largest absolute value of a matrix's eigenvalues. It's computed by finding all eigenvalues of the matrix and then taking the maximum of their absolute values. For a NSFD scheme, the spectral radius is applied to the Jacobian matrix of the discrete system. If $\mathscr{R}(J) < 1$, the NSFD scheme is considered stable, meaning the numerical solution will not grow unbounded over time. Thus, we solve the characteristic equation for the stability of the eigenvalues λ_1, λ_2 and λ_3. The specific conditions for stability will depend on the φ, $\delta, \zeta, \rho, \omega, \theta, \psi, \pi, \phi, \zeta, \upsilon, \Lambda$ and η parameters and the control variables (U, V and W).

Observe that the spectral radius of the Jacobian matrix J for each time step "h" such that $0 < h < 1000$, as shown in Figure 2, remains less than unity for each time step. The spectral radius of a matrix is the largest absolute value of its eigenvalues. For the Jacobian matrix J, which represents the linearisation of the system of equations around an equilibrium point, the spectral radius is a

key factor in determining the stability of the numerical method. Since the analysis is done for different time steps h within the range $0 < h < 1000$, then the time step h controls the discretisation of time.

The spectral radius in Figure 2 gives an insight into the behavior of $\lambda_i, i \leq 3$ and the information of whether J is stable or not. If $\mathscr{R}(J)$ is the spectral radius of J based on λ_i, then

$$\mathscr{R}(J) = \underset{1\leq i\leq n}{\text{maximise}}\{|\lambda_1|, \cdots, |\lambda_n|\}. \tag{20}$$

If $\mathscr{R}(J) < 1$, then the system is stable, otherwise unstable. Thus, the spectral radius is fundamentally tied to the eigenvalues of a matrix, providing insights into the behavior of the matrix in iterative processes and stability. As shown in Figure 2, $\mathscr{R}(J) < 1$ indicates that all eigenvalues of the Jacobian matrix J lie within the unit circle of radius 1 centred at the origin in the complex plane. This is a necessary condition for the stability of the NSFD scheme. Therefore, since the spectral radius of the Jacobian matrix is less than one for each time step, it implies that the NSFD scheme is convergent.

In other words, the numerical solution will approach the true solution as the time step progresses without becoming unbounded or oscillating unstably. By performing this stability analysis at the equilibrium state of the WES model, we confirm that the numerical scheme will accurately simulate the behaviour of the WES system near this equilibrium.

4 | Simulation Results and Discussions

To evaluate the performance of the proposed WES model described in Equations (3a–c), we implement two numerical schemes using parameter values outlined in Table 2a and initial values $X(0) = 5.5$, $Y(0) = 20000$ and $Z(0) = 2.74$; NSFD and RK4. The initial values used in our simulations, $X(0) = 5.5$, $Y(0) = 20{,}000$, and $Z(0) = 2.74Z$, were chosen as baseline assumptions to test the model's feasibility and stability rather than as direct field data. For carbon sequestration, 5.5 represents a sequestration index consistent with reported rates of $4.5 - 40.7\ tCO_2/ha/year$ in European forests [34]. The assumed 20,000 visitors reflect annual recreation levels within the predicted range of $15{,}000 - 24{,}000 visits/ha/year$ [35, 36]. For water filtration, the baseline 2.74 aligns with mid-range Water Quality Index values observed in moderately impacted European rivers [36], with future calibration planned using local field data. The simulations were executed on optimized AWS EC2 instances (C5 series), using MATLAB 2025b, configured for high performance numerical simulation. We employed the NSFD method and RK4 scheme to solve the model equations. Their performance is compared using the parameter values from Table 2a. The evaluation of the proposed WES model was conducted under three distinct control regimes: high, moderate and low, with their respective control parameters summarized in Table 2b.

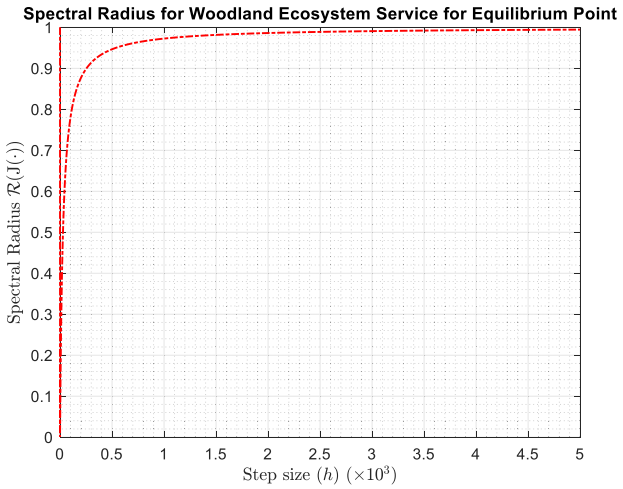

FIGURE 2 | Spectral radius for the woodland ecosystem equilibrium point.

The wide variation observed in parameters such as δ, π, and η across the high, medium, and low scenarios (Tables 2a and 2b) reflects the use of extreme but ecologically plausible ranges to evaluate the robustness of the model. Ecological systems are inherently nonlinear and regime-dependent, where dissipation rates, productivity indices, and efficiency coefficients can vary by several orders of magnitude depending on disturbance levels, nutrient availability, or land-use intensity. For instance, sensitivity analyses of ecosystem productivity models have shown that parameters linked to respiration, biomass allocation, and turnover can dominate system dynamics and shift considerably under different environmental conditions [37, 38]. Similarly, cross-site comparisons of carbon cycle models demonstrate that parameter values often require scaling to capture ecosystem responses across contrasting climatic and stress regimes [39, 40].

The NSFD method was adopted to address the nonlinearity problems of the WES model without compromising stability. WES follows conservation laws, and the NSFD method is particularly well-suited for long-term studies that uphold these laws. In contrast, while RK4 offers high accuracy in the short term, it is not well-suited for nonlinear systems and may not consistently preserve the conservation properties of WES. For this reason, RK4 serves as a reference baseline in this study to assess the conservation performance of the NSFD method. A limitation of this study is the use of fixed parameter values for simulation. Future researchers may adjust these parameters based on the specific country or community being investigated.

TABLE 2a | Performance evaluation parameter values for the WES.

Parameters	$\varphi \times 10^{-4}$	$\delta \times 10^{-5}$	$\zeta \times 10^{-4}$	$\rho \times 10^{-4}$	$\psi \times 10^{-3}$	π	$\omega \times 10^{-2}$	ϕ	$\Lambda \times 10^{-2}$	$\eta \times 10^{-3}$	$\theta \times 10^{-7}$	$\upsilon \times 10^{-4}$
High	274	5480	548	13.7	2	2	5	0.2	30	500	825	275
Moderate	274	5.48	548	137	2	1	5	0.2	30	5	825	275
Low	2.74	0.548	548	137	2	0.1	5	0.2	0.3	0.005	825	275

TABLE 2b | Control parameter values for the WES.

Parameters	γ	K_1	K_2	K_3	K_4	K_5	α_1	α_2	α_3	α_4	ε	σ
High	0.0275	130.9	450	130.9	450	505	1	1	1	1	0.075	0.053
Moderate	0.0275	130.9	450	130.9	450	505	1	1	1	1	0.075	0.053
Low	0.0275	130.9	450	130.9	450	505	1	1	1	1	75	0.053

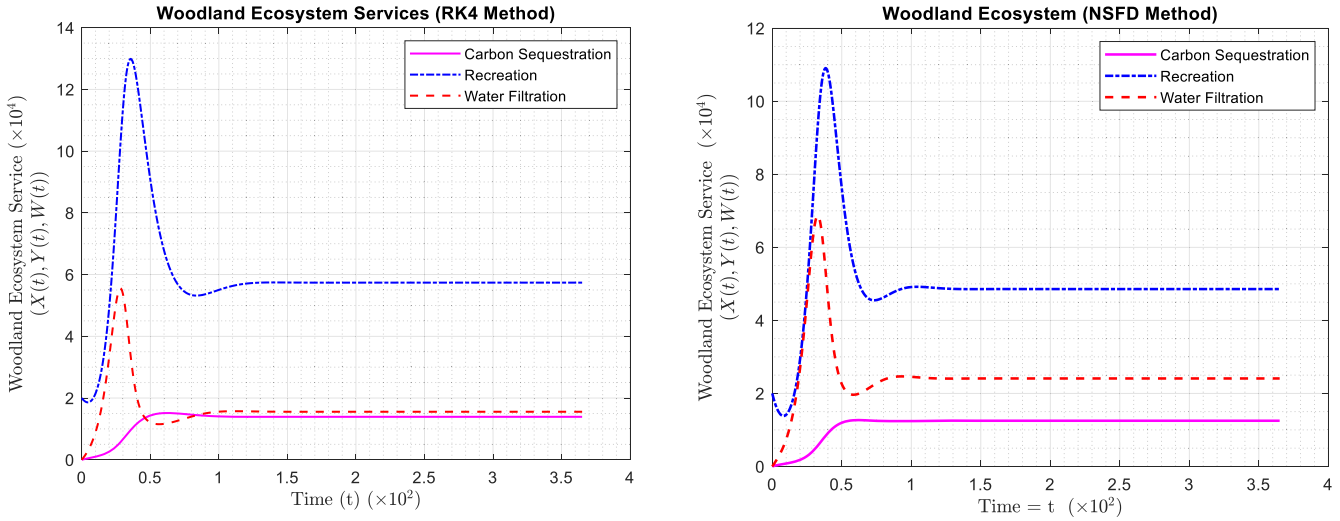

FIGURE 3 | Dynamics of system model Equations (3a–c) with high control parameters $\delta = 5.48 \times 10^{-2}$ (effectiveness of reforestation efforts), $\pi = 2.0$ (Control coefficient for recreational infrastructure development) and $\eta = 0.5$ (Control coefficient for water conservation efforts) using RK4 and NSFD Schemes.

4.1 | WES Model Under High Control Parameter Value ($\delta = 0.0548$, $\pi = 2$ and $\eta = 0.5$)

Following Equations (3a–c) and control variables in Equations (2a–c), the results presented in Figure 3 illustrate the performance of the proposed WES under high reforestation effectiveness, recreational infrastructure development, and water conservation efforts. This was evaluated using both the RK4 and NSFD methods. Initially, both models show an increase in recreation and water filtration services, followed by a decline and eventual stabilization. This trend suggests that significant investments in these areas lead to initial service improvements. However, the subsequent decline may indicate diminishing returns or the overextension of resources, which could strain the ecosystem. The eventual stabilization points to the ecosystem's adjustment to a new equilibrium, where services are maintained at a sustainable level. As observed, the strong overlap between recreation and water filtration highlights their interdependence. In the NSFD model, both services stabilize together, reflecting how effective management promotes a balanced distribution of resources. The RK4 model, on the other hand, highlights the close relationship between carbon sequestration and water filtration, suggesting that improvements in water quality and carbon sequestration enhance soil and plant health. Despite the lower values compared to water filtration, carbon sequestration remains stable, signaling that the ecosystem prioritizes water filtration and recreation. In the NSFD model, carbon sequestration consistently ranks lower, implying that water quality and recreation are given more attention than carbon storage. This outcome raises concerns about the need to reassess conservation priorities, especially if long-term carbon storage is a key objective.

Figure 4a–c reveals that high effectiveness in reforestation, recreational infrastructure, and water conservation leads to complex interactions between ecosystem services. The differences between RK4 and NSFD methods emphasize the importance of using various modeling approaches to evaluate management practices. The key takeaway is that enhancing one service requires careful monitoring of others to ensure the ecosystem remains balanced and sustainable.

The higher values for carbon sequestration, recreation, and water filtration in the RK4 method compared to the NSFD method, as shown in Figure 4a–c can be explained by differences in how these numerical methods address the dynamics of the WES model.

RK4, being a higher-order numerical method, provides greater accuracy and precision in approximating differential equations. It excels in predicting smooth and well-behaved systems, often leading to higher variable estimates. The high accuracy of this method can sometimes overestimate values, especially in complex, nonlinear systems like ecosystems, where small fluctuations or dynamics can amplify growth. In contrast, NSFD methods prioritize preserving the system's qualitative features, such as non-negativity and boundedness, but do so conservatively. This approach can lead to lower carbon sequestration, recreation,

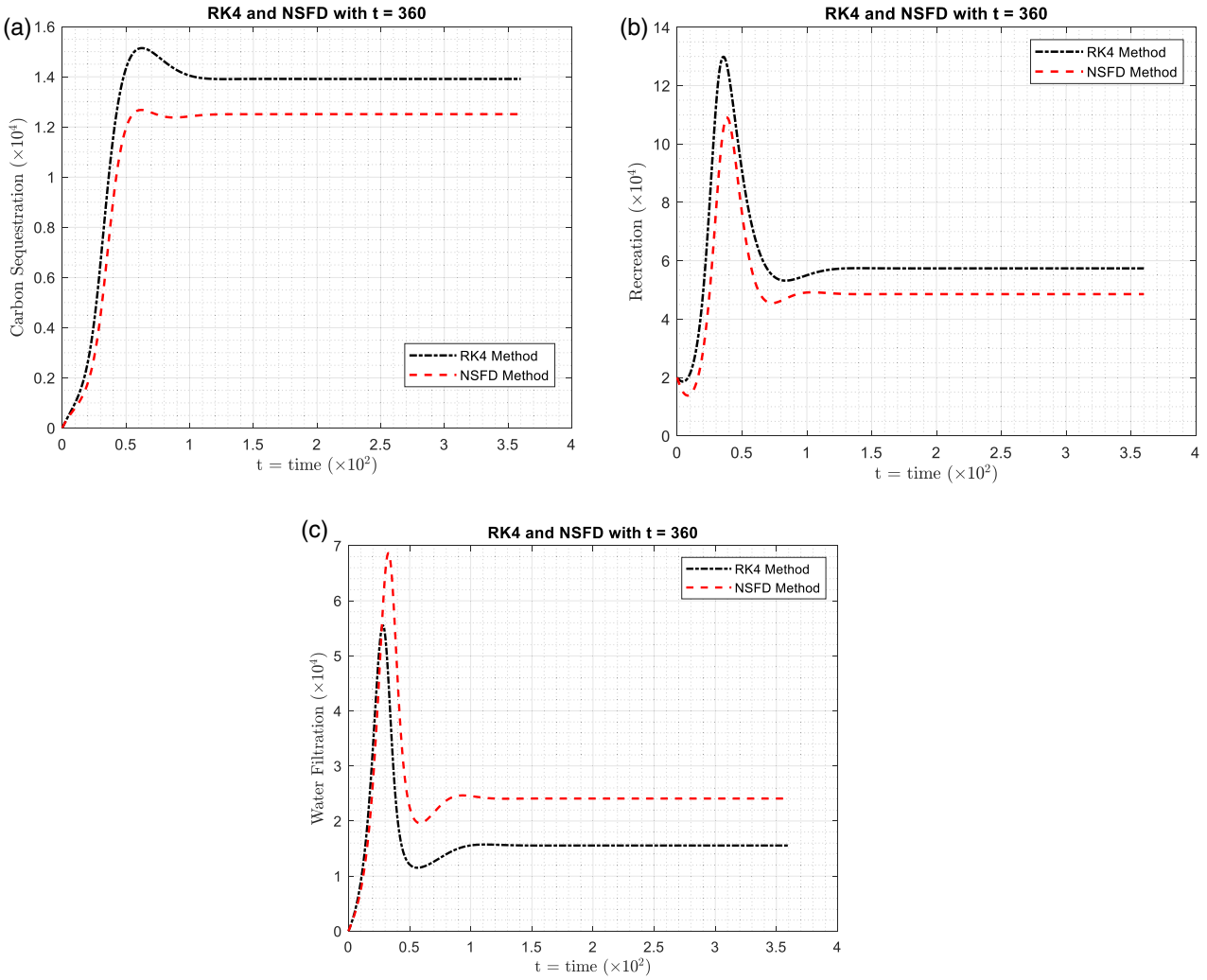

FIGURE 4 | (a) Dynamics of carbon sequestration ($\delta = 5.48 \times 10^{-2}$, $\pi = 2.0$ and $\eta = 0.5$ using RK4 and NSFD schemes). (b) Dynamics of recreation ($\delta = 5.48 \times 10^{-2}$, $\pi = 2.0$ and $\eta = 0.5$ using RK4 and NSFD schemes). (c) Dynamics of water filtration ($\delta = 5.48 \times 10^{-2}$, $\pi = 2.0$ and $\eta = 0.5$ using RK4 and NSFD schemes).

and water filtration estimates as it smooths out fluctuations that might otherwise increase these values. While NSFD methods are generally more stable for long-term simulations, their conservative nature can result in less pronounced increases in these variables. When control coefficients, representing reforestation, recreational infrastructure, and water conservation efforts, are high, the system's sensitivity to changes increases. RK4's precision captures these sensitivities, translating into higher values for ecosystem services. NSFD methods, though responsive, provide a more tempered response, resulting in less dramatic increases. In other words, NSFD should be applied in the first instance, global and long-term explorative investigation of ecosystem services of any location while RK4 should be deployed for short-term and detailed investigations of ecosystem services performances of the sites.

The WES model likely involves nonlinear interactions among carbon sequestration, recreation, and water filtration. RK4's accuracy in tracking these interactions can lead to higher peaks due to its ability to capture positive feedback loops or synergistic effects. Conversely, NSFD might dampen these interactions, leading to lower but more stable values. RK4 often uses smaller time steps to achieve its high accuracy, enabling it to capture rapid changes and variations in the system, resulting in higher values for ecosystem services. NSFD methods may use larger or variable time steps, smoothing out rapid fluctuations and producing lower overall values. The higher values in RK4 might suggest that the system is nearing an upper limit or reflecting a more optimistic scenario under given control efforts. These predictions, however, may be more sensitive to initial conditions and parameter choices. The lower values in NSFD likely represent a more cautious long-term prediction, indicating a more sustainable outcome where the system stabilizes without overshooting.

4.2 | WES Model Under Moderate Control Parameter Value ($\delta = 5.48 \times 10^{-5}$, $\pi = 1$ and $\eta = 5 \times 10^{-3}$)

The analysis of Figure 5 illustrates the dynamics of a woodland ecosystem under moderate reforestation, recreational infrastructure development, and water conservation efforts over time

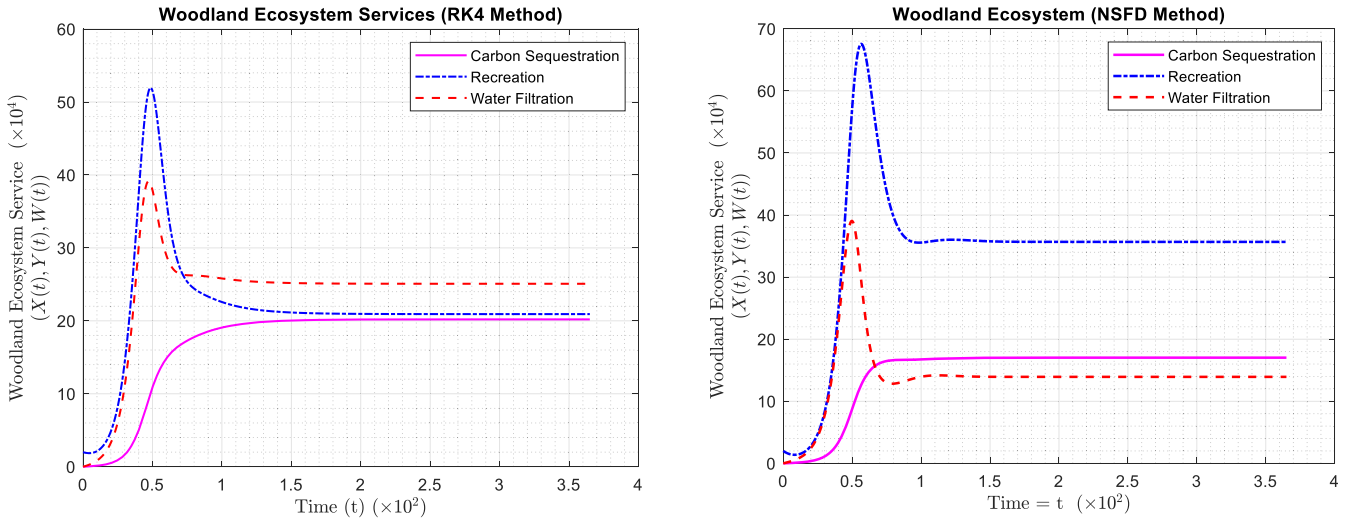

FIGURE 5 | Dynamics of model Equations (1a–c) with moderate control parameters $\delta = 5.48 \times 10^{-5}$(effectiveness of reforestation efforts), $\pi = 1.0$ (Control coefficient for recreational infrastructure development) and $\eta = 5 \times 10^{-3}$ (Control coefficient for water conservation efforts) using RK4 and NSFD schemes ($t = 360$).

(t = 360). Using the RK4 and NSFD methods, the system's behavior shows slight variations, though both methods reveal how moderate interventions enhance carbon sequestration, recreation, and water filtration in a balanced way, preventing overuse or degradation.

Recreation and water filtration both peak in response to these moderate efforts, with recreation rising higher due to the immediate impact of infrastructure improvements. After peaking, both services decline, reflecting the ecosystem's natural limits and resource consumption patterns. In RK4, the intersection of recreation and water filtration reveals critical moments where the ecosystem's capacity for water filtration aligns with recreational use, highlighting the need to safeguard water quality as human activity increases. Carbon sequestration, while increasing modestly in both methods, stabilizes over time. This reflects the slower and more gradual nature of carbon storage processes, which are enhanced but not overstressed under moderate control values. These moderate interventions allow the ecosystem to support multiple services without overwhelming any one area.

The intersections observed in RK4 demonstrate that the ecosystem efficiently manages resources, with different services becoming dominant at different times. This balance prevents any single service from overwhelming the system. For example, the trade-offs between recreation and water filtration indicate that while recreational infrastructure improves, it may impact water quality. Effective management of these trade-offs is essential to sustain both services and avoid compromising the ecosystem's health. Similarly, the intersection between water filtration and carbon sequestration underscores their interconnectedness. Healthy forests that sequester more carbon may also improve water quality, but maintaining balance is crucial to prevent any unintended effects. The simulation result highlights the importance of adaptive management practices. Ecosystem managers should regularly monitor and adjust interventions to maintain balance among services [41]. Recognizing when and where key intersections occur between services can guide management actions, such as increasing water conservation when recreational activities threaten to reduce water quality. Stabilizing services, particularly carbon sequestration, is vital for the long-term resilience of the ecosystem. By maintaining moderate control values, the ecosystem can sustainably support diverse services without risking long-term degradation.

Figure 6a–c illustrate how two numerical methods, the RK4 method and the NSFD method, handle the dynamics of a woodland ecosystem under moderate conditions, focusing on the effectiveness of reforestation, recreational infrastructure development, and water conservation efforts. These methods exhibit distinct behaviours in predicting Ess, especially when control coefficients are set at moderate levels.

RK4, a higher-order and more precise method, is particularly sensitive to initial conditions and moderate parameter changes. This sensitivity enables RK4 to capture subtle positive feedback loops, leading to potentially higher predictions for carbon sequestration. In contrast, NSFD tends to smooth out such dynamics, providing a more conservative estimate of carbon sequestration. As a result, RK4 might show a greater accumulation of carbon stock over time compared to NSFD, which might underpredict this accumulation due to its conservative nature. When assessing the effectiveness of recreational infrastructure, RK4 might reflect lower values because it captures small fluctuations or dampens oscillations that can occur with moderate investments in recreation. This damping effect results in lower overall recreational values in RK4.

On the other hand, NSFD, which emphasizes stability and the preservation of qualitative features, might not dampen these fluctuations as much, leading to a higher estimate of recreational value. NSFD allows for a more gradual and sustained increase in recreational benefits, providing a different perspective on the impact of moderate infrastructure development. RK4 also highlights the more prominent interaction between recreation and other variables, such as carbon sequestration and water filtration.

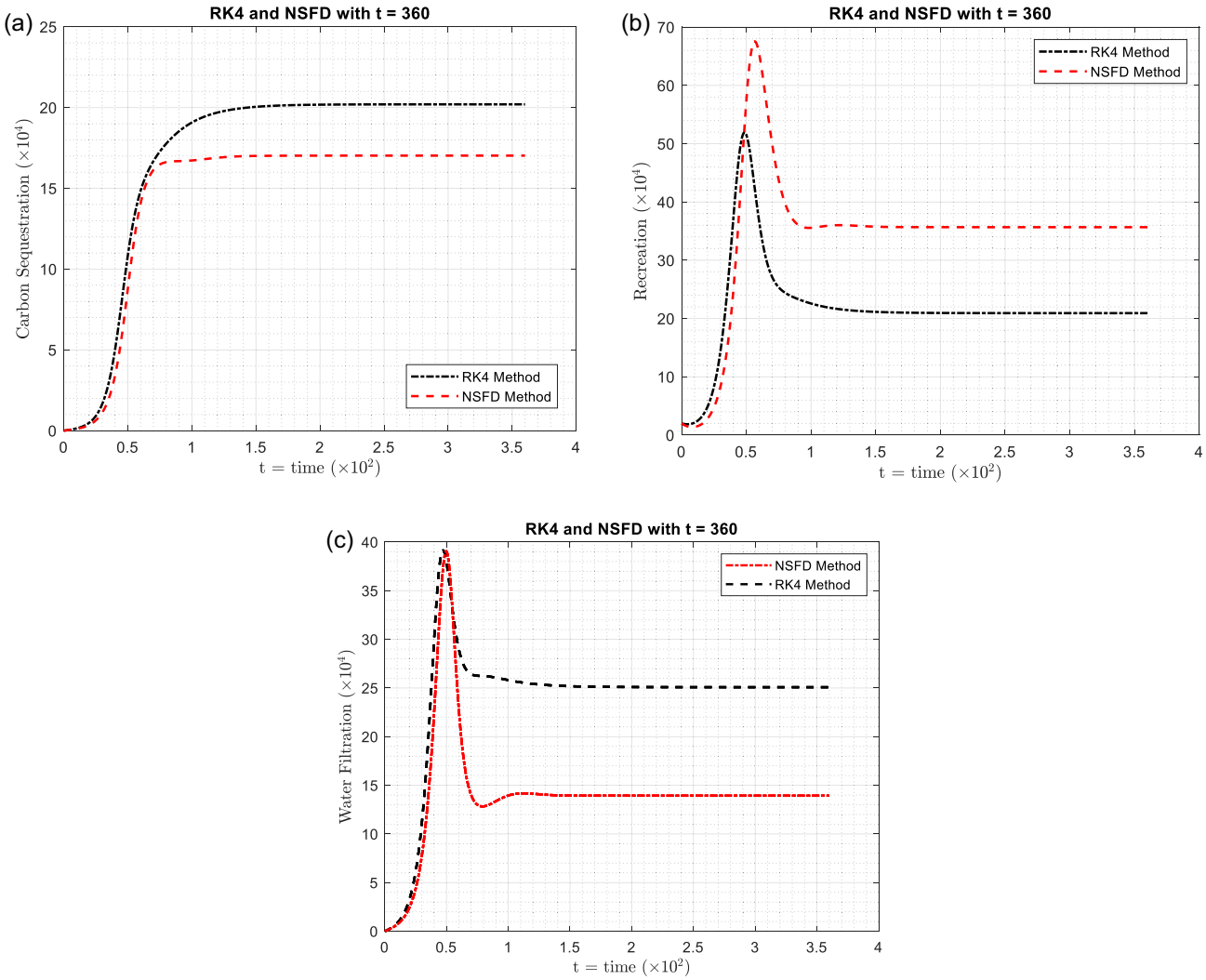

FIGURE 6 | (a) Dynamics of carbon sequestration ($\delta = 5.48 \times 10^{-5}$, $\pi = 1.0$ and $\eta = 5 \times 10^{-3}$ using RK4 and NSFD schemes). (b) Dynamics of recreation ($\delta = 5.48 \times 10^{-5}$, $\pi = 1.0$ and $\eta = 5 \times 10^{-3}$ using RK4 and NSFD schemes). (c) Dynamics of water filtration ($\delta = 5.48 \times 10^{-5}$, $\pi = 1.0$ and $\eta = 5 \times 10^{-3}$ using RK4 and NSFD schemes).

If moderate control values lead to competition between these services, RK4 might reflect this competition more accurately, showing a lower recreation value for urban communities.

In contrast, NSFD might handle these interactions more smoothly, resulting in a higher recreation value as it balances the trade-offs between different ecosystem services. Water filtration appears to be less sensitive to moderate changes in control coefficients compared to carbon sequestration and recreation.

Consequently, both RK4 and NSFD methods may predict similar outcomes for water filtration under moderate effectiveness values. The stability and linearity of the factors influencing water filtration could lead to convergence in the predictions of both methods, as the natural capacity of the ecosystem to filter water remains relatively constant. Under moderate control coefficients, the system's response tends to be more linear and less extreme, which can reduce the differences between numerical methods. While RK4 might show slightly higher or lower values depending on how it handles dynamic responses, NSFD tends to produce more consistent results across different levels of control effectiveness. Overall, the differences between RK4 and NSFD are more pronounced for services like carbon sequestration and recreation, while they converge for more stable services like water filtration.

4.3 | WES Model Under Low Control Parameter Value ($\delta = 548 \times 10^{-8}$, $\pi = 0.1$ and $\eta = 5 \times 10^{-6}$)

When the effectiveness of reforestation efforts, recreational infrastructure development, and water conservation measures are set to very low values, the dynamics of the woodland ecosystem change significantly, as displayed in Figure 7 with $t = 100$ and 360 and also in Figure 8. This leads to the observed behaviors in water filtration, carbon sequestration, and recreation in the NSFD and RK4 methods.

Figure 7 shows that low reforestation results in a minimal increase in carbon stock. Trees and other vegetation, which are primary agents of carbon sequestration, grow slowly or not at all. As a result, carbon sequestration increases only slightly at

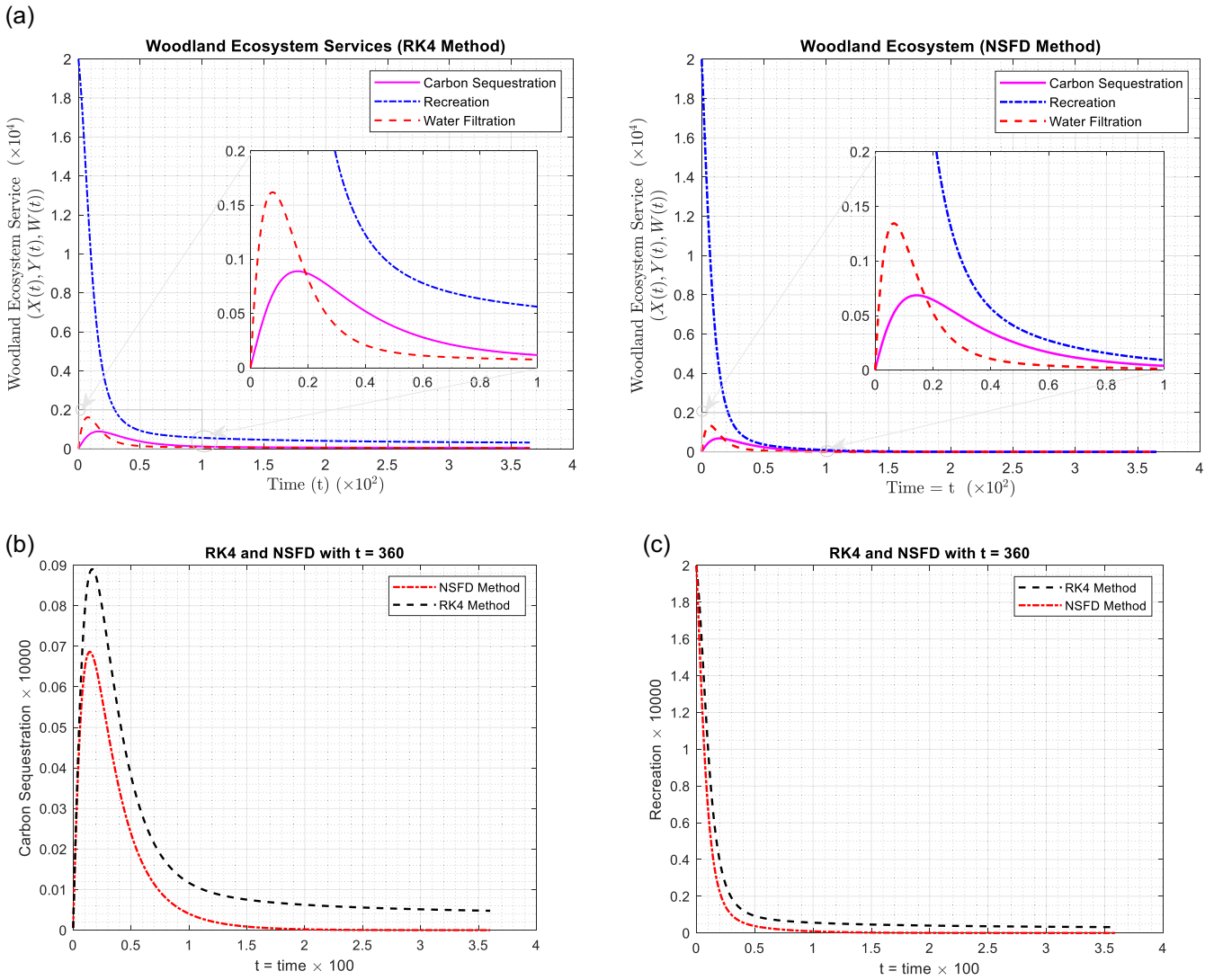

FIGURE 7 | (a) Dynamics of model Equations (1a–c) with low control parameters $\delta = 548 \times 10^{-8}$ (effectiveness of reforestation efforts $U(t)$ on increasing carbon stock), $\pi = 0.1$ (Control coefficient for recreational infrastructure development $V(t)$ on recreational value) and $\eta = 5 \times 10^{-6}$ (Control coefficient for water conservation efforts $W(t)$ on water quality) using RK4 and NSFD schemes ($t = 360$). (b) Dynamics of carbon sequestration when $\delta = 5.48 \times 10^{-6}$, $\pi = 0.1$ and $\eta = 5 \times 10^{-6}$ using RK4 and NSFD schemes. (c) Dynamics of recreation when $\delta = 5.48 \times 10^{-6}$, $\pi = 0.1$ and $\eta = 5 \times 10^{-6}$using RK4 and NSFD schemes.

first, as existing vegetation still sequesters some carbon, but without sufficient reforestation, this service cannot sustain itself and begins to decline, eventually stabilizing near zero. When the control coefficient for recreational infrastructure is very low, it means that investments in enhancing recreational facilities and experiences are minimal. Recreation might initially start at a certain level due to existing infrastructure, but with little to no new investment, the quality and appeal of recreation decrease over time. In the NSFD method, this decline starts from the initial value, reflecting the lack of enhancement in recreational opportunities. Similarly, low effectiveness in water conservation efforts means that the ecosystem's ability to filter water is not significantly enhanced. Initially, the natural capacity of the ecosystem to filter water might lead to a small increase in water filtration, but without additional conservation measures, this capacity is quickly exhausted, leading to a decline and stabilization near zero.

Figures 7b,c and 8 demonstrate the specific behaviors of the two methods on carbon sequestration, recreation and water filtration in a woodland ecosystem. The NSFD method is designed to preserve the qualitative behavior of the system, even under low control effectiveness. This method tends to smooth out fluctuations and avoid extreme changes, leading to a gradual decline in all services. As carbon sequestration, water filtration, and recreation decline, they eventually converge near zero, with water filtration and carbon sequestration overlapping as they stabilize. This overlap occurs because, at very low control effectiveness, both services are equally minimal, and the method's conservative nature causes them to follow similar trajectories. RK4, being more sensitive to initial conditions and dynamic changes, captures the interaction between carbon sequestration and water filtration more distinctly. It shows these services increasing slightly and then overlapping as they decline and stabilize.

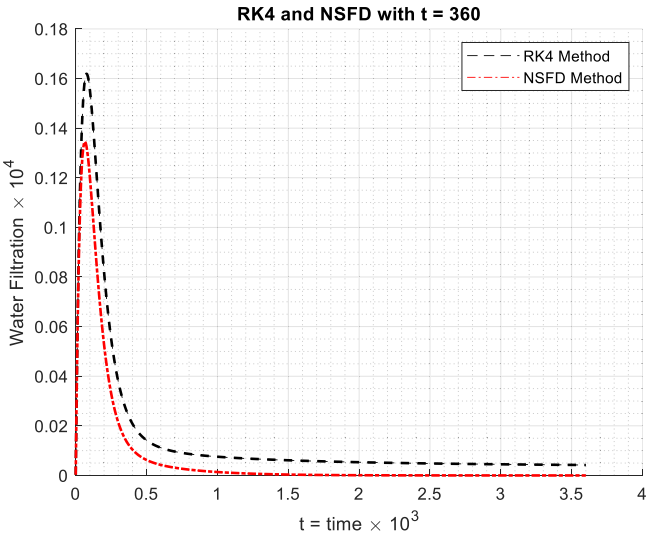

FIGURE 8 | Dynamics of water filtration ($\delta = 5.48 \times 10^{-6}$, $\pi = 0.1$ and $\eta = 5 \times 10^{-6}$ using RK4 and NSFD schemes).

However, RK4 also highlights that, due to the minimal impact of low recreational investment, recreation may not follow the same trajectory as carbon sequestration and water filtration, leading to a situation where only carbon sequestration and water filtration overlap. In the RK4 method, recreation does not overlap with carbon sequestration and water filtration because the method captures the independent decline of recreation more distinctly due to the low control coefficient. Since recreational activities are often more directly impacted by infrastructure and investment, the lack of these enhancements leads to a separate and more pronounced decline in recreation, while carbon sequestration and water filtration driven more by natural processes follow a different, albeit connected, path.

4.4 | Benefits of the Proposed Model

In Section 2, we developed an analytical model in Equations (3a–c) for evaluating the WES that captures the control parameters for adapting the model into specific locations. Multiregional studies can be explored by combining the proposed compartmental model with the Leontief Input–Output model presented in [23]. Based on Equations (3a–c) and the control parameters in Equations (2a–c), natural capital accounts for different national governments can be easily prepared. While the lessons learned from one ecosystem services site might inform useful study parameters for other sites, cross-site comparisons often imply that parameter values require scaling to capture ecosystem responses across contrasting climatic and stress regimes [39, 40]. As the UK continues to deepen its investment into natural capital accounting, new entrant countries could scale their natural accounting systems based on the UK framework. The WES model developed in this study provides a platform on what parameters to look for in preparing WES and capital accounts. Although the use of compartmental modelling already exists in agriculture and chemical engineering, based on the present study, compartmental modelling can be extended to computer networks and electrical power systems where each of the generators and loads can be modelled as compartments.

This study highlights the critical role of data-driven, evidence-based policymaking in optimizing natural capital management for sustainable urban development. For example, Figures 3–8 demonstrate the strong link between smart city governance and ecosystem services, emphasizing their importance in driving innovative approaches to urban sustainability [42]. Aligned with the UK's 2035 growth agenda and commitment to a net-zero transition [43], our work argues that effective policy must balance immediate ecological needs with long-term benefits. Interventions in reforestation, recreational infrastructure, and water conservation should support both environmental sustainability and socioeconomic resilience. For example, some UK water sites are being plagued by micro-particles, antifouling chemicals and physical disturbances from recreational fiberglass boats abandoned in the waterbodies reducing the physical flow, recreational attraction, tourism and monetary value of UK water bodies. The water pollution from these fiberglass boats heavily impacts oysters, mussels, and other invertebrates responsible for natural water filtration, nutrient cycling, water quality, and maintaining water clarity. While recreational boats should not be discouraged, environmental policies should be enacted to balance using recreational boats (that meet specific environmental qualities) and preserving water quality and the ecosystems services provided by freshwater. Our study therefore can be used to evaluate the impacts of these specific control parameters for short-term (using RK4 method) and long-term (using NSFD method) on ecosystem services and natural capital accounting.

Given the problem of water pollution, as an example, this study can be extended to investigate the roles of game theory as a win-win approach to encouraging environmentally friendly practices for recreational boat users, tourists, and local communities around rivers, lakes, and other waterbodies.

In this regard, AI and digital innovation are key enablers in advancing smart social infrastructure and the UK's natural capital strategy. Specifically:

- Reforestation increases carbon sequestration, supports climate regulation, and creates green jobs in agriculture and forestry.
- Recreational infrastructure, including well-designed parks and public green spaces, enhances physical and mental health, strengthens social cohesion, and promotes equitable urban living.
- Water conservation ensures sustainable clean water supply, reduces health risks, and improves community resilience against climate-related disruptions.

To ensure fair access and lasting impact, policymakers must prioritize inclusivity in natural capital initiatives. Incorporating data governance principles, such as data quality, security, and ethics, strengthens environmental monitoring, predictive analytics, and resource management. Model simulations in Section 4 show that targeted adjustments in management parameters produce distinct ecosystem outcomes. For example, increasing δ boosts carbon sequestration and water quality, supporting afforestation and watershed protection policies. Raising π improves recreational value but may reduce long-term ecosystem stability, indicating

that recreation policies must balance human use with ecological limits. Higher η enhances water filtration and indirectly stabilizes other ecosystem services, highlighting the value of integrated conservation strategies. These results provide computational evidence that the most sustainable policy pathway combines a coordinated increase in δ and η with a regulated π. This approach optimizes multi-service ecosystem performance and enables adaptive, transparent, and efficient policy implementation. Overall, the findings underscore the need for integrated policies linking reforestation, sustainable infrastructure, and water conservation to strengthen urban resilience. By embedding natural capital ecosystem services into smart city governance frameworks, cities can improve environmental outcomes, enhance human well-being, and secure a sustainable, liveable future for generations.

4.5 | Discussion and Policy Implications

This study develops a WES model to support natural capital planning in sustainable cities by analyzing carbon sequestration, recreation, and water filtration using NSFD and RK4 numerical schemes. The results demonstrate that reforestation intensity is the primary driver of long-term carbon sequestration in urban woodlands. Increasing the reforestation control leads to higher equilibrium carbon stocks, indicating enhanced long-term carbon storage and improved climate change mitigation potential. The RK4 method captures more rapid and pronounced carbon accumulation due to its higher sensitivity to dynamic changes and initial conditions, whereas the NSFD method provides smoother, more conservative trajectories that better reflect gradual ecosystem adaptation under long-term management.

The control variables representing reforestation, recreational infrastructure development, and water conservation effectively quantify policy-driven interventions at high, moderate, and low levels of effectiveness. Investment in recreational infrastructure produces sustained growth in the recreation state variable, translating into improved accessibility, increased outdoor participation, and wider social and public health benefits in urban environments. Strong water conservation measures significantly enhance water filtration capacity, leading to improved water quality and overall ecosystem health. Over time, both numerical methods converge in their predictions as water filtration stabilises, highlighting the long-term sustainability of these services once effective management practices are in place. The variation in outcomes across different control levels has clear policy relevance. High control effectiveness delivers strong and lasting improvements across all ecosystem services, reflecting robust and sustained policy commitment. Moderate effectiveness results in steady, resilient growth that aligns with practical resource constraints and long-term planning objectives. In contrast, low effectiveness leads to minimal gains followed by decline and stabilization at near-zero service levels, indicating insufficient investment and weak policy enforcement. From a policy perspective, these findings emphasize the importance of coordinated woodland strategies that integrate reforestation, sustainable recreational development, and water conservation to maximize natural capital benefits in urban settings.

4.6 | WES Model Limitations

There are some limitations that should be considered when interpreting the results in practice. First, the simulations employ fixed parametric values, which is common in computational modeling. However, ecosystem service dynamics vary across locations due to site-specific ecological, climatic, and socio-economic conditions. As such, users seeking to apply the model in other contexts should undertake appropriate parameter calibration to reflect local conditions. Second, the model is formulated using nonlinear interactions with integer-order derivatives, which limits its ability to capture memory effects, time delays, and long-term dependencies that are characteristic of many ecological processes. In addition, uncertainty is not explicitly represented, as stochastic components and sensitivity analyses were not incorporated. Consequently, uncertainties arising from model inputs, sensor measurements, and inherent ecosystem response variability are outside the current scope. Finally, the governance and control scenarios are conceptual and assume full effectiveness of policy interventions related to reforestation, recreation, and water conservation. In real-world settings, such interventions are often constrained by social, economic, institutional, and policy factors, which may influence their actual impact on woodland ecosystem services.

4.7 | Future Direction

Ongoing work aims to enhance scalability and real-world applicability by extending the model's structural, numerical, and policy relevance. Adaptive parameters will evolve with changing ecological and socio-economic conditions, improving realism and enabling robust scenario-based forecasting. Fractional-order modeling is explored to capture memory effects and long-term dependencies in woodland ecosystem processes. Monte Carlo uncertainty and sensitivity analyses benchmark model stability under varying initial conditions and inputs. Further developments include agent-based hybrid modeling to simulate human-environment interactions and governance-driven land-use policies. Geographic Information System (GIS)-based spatial integration captures heterogeneity and simulates ecosystem services at finer, region-specific scales, validated against historical intervention data. Optimal control techniques support budget-constrained, multi-stakeholder decision-making, while human-in-the-loop behavioral factors better represent participation in conservation and recreational activities. Extensions also cover stochastic dynamics, networked system generalizations, and regime-switching formulations. These are contextualized within relevant frameworks, including Input–Output Analysis, Game Theory, the Gene–Environment model, and Homogenization Theory. Overall, these efforts strengthen intersections with existing studies and enhance the model's applicability to real-world urban woodland management and policy design.

5 | Conclusion

This study demonstrates the value of a quantitative WES modeling for evaluating woodland natural capital in sustainable cities. By combining NSFD and RK4 numerical schemes, the model captures both short-term ecosystem responses and long-term

equilibrium behavior, offering complementary insights that single-method approaches cannot. Strong reforestation policies are shown to enhance carbon sequestration, while balanced investment in recreational infrastructure and effective water conservation strengthens ecosystem services, public well-being, and urban sustainability. Compared with existing approaches, this model integrates multiple ecosystem services, policy-driven control variables, and numerical sensitivity, allowing more realistic, adaptable, and scenario-based assessment of urban woodlands. RK4 captures rapid ecosystem responses, while NSFD provides stable long-term projections, together supporting more informed, evidence-based decision-making. Future work will extend the model to incorporate stochastic dynamics, networked ecosystem interactions, regime-switching behavior, optimal control strategies, and human behavioral effects, improving realism and applicability. Overall, this approach provides policymakers with a robust tool to optimize natural capital, enhance urban resilience, and implement sustainable city strategies more effectively than previous models.

Author Contributions

Kennedy Chinedu Okafor: conceptualization, writing – original draft, methodology, data curation, validation, project administration. **Omowunmi Mary Longe:** writing – review and editing, supervision, validation, data curation.

Acknowledgments

The simulation scripts and configurations executed on AWS EC2 instances are available from the corresponding author on reasonable request, subject to institutional data-sharing policies and non-disclosure agreements. The authors gratefully acknowledge the invaluable support of the Office for National Statistics (ONS), UK, and the Natural Capital Accounts Projects Team within the Environment Division, particularly for their contributions to the Woodland Natural Capital Accounts 2024 and the UK Natural Account 2023. We also extend sincere thanks to our former ONS colleagues—Maggie MacLellan, Dr. Hazel Trenbirth, and Dr. Oluwafisayo Alabi—whose early contributions significantly enriched this work. Special appreciation is due to Tristan John Pett and Ellen Clowser for their exceptional input and collaborative support.

Funding

This work was supported in part by the Department of Engineering, Manchester Metropolitan University, UK. Tertiary Education Trust Fund (TETF/ES/UNIV/IMO STATE/TSAS/2021).

Conflicts of Interest

The authors declare no conflicts of interest.

Data Availability Statement

The data that support the findings of this study are available on request from the corresponding author. The data are not publicly available due to privacy or ethical restrictions.

Peer Review

For transparency, the peer review documents associated with this article are available at https://doi.org/10.1002/eng2.70732.

References

1. NatureScot, "Ecosystem Services - Nature's Benefits. Scotland's Nature Agency," 2020.

2. X. Dong and M. Liu, "Relationships Among LUCC, Ecosystem Services and Human Well-Being," *Journal of Beijing Normal University(Natural Science)* 58, no. 3 (2022): 465–475, https://doi.org/10.12202/j.0476-0301.2022115.

3. X. Chen, H. Li, W. Zhang, and X. Ge, "The Impact of Land Use Transition on Ecosystem Service Value in Lixiahe Area: Multi-Scenario Simulation Based on Markov-FLUS Model," *Resources Science* 47 (2025): 182–195, https://doi.org/10.18402/resci.2025.01.14.

4. L. Fu, Y. Ren, L. Lu, and H. Chen, "Relationship Between Ecosystem Services and Rural Residential Well-Being in the Xin'an River Basin, China," *Ecological Indicators* 140 (2022): 108997.

5. M. MacLellan, H. Trenbirth, and K. C. Okafor, *UK Natural Capital Accounts: 2023*, ed. O. f. N. Statistics (UK Government, 2023).

6. G. Valatin and J. Starling, "Valuation of Ecosystem Services Provided by UK Woodlands," UK NEA Economic Analysis Report, 2010.

7. B. Döhring, A. Hristov, A. Thum-Thysen, and C. Carvell, "Reflections on the Role of Natural Capital for Economic Activity," European Economy-Discussion Papers, 2023.

8. R. Costanza, R. d'Arge, R. De Groot, et al., "The Value of the World's Ecosystem Services and Natural Capital," *Nature* 387 (1997): 253–260.

9. J. Philips, "Principles of Natural Capital Accounting," UK Office for National Statistics, 2017.

10. K. Leach, A. Grigg, B. O'Connor, et al., "A Common Framework of Natural Capital Assets for Use in Public and Private Sector Decision Making," *Ecosystem Services* 36 (2019): 100899, https://doi.org/10.1016/j.ecoser.2019.100899.

11. Department for Environment, Food & Rural Affairs, "Enabling a Natural Capital Approach (ENCA): Guidance," GOV.UK Updated February 4, 2025.

12. J. Ravetz, "Future of the Urban Environment & Ecosystem Services in the UK," in *Future of Cities Foresight Programme* (Government Office of Science, 2015).

13. R. Giffinger, C. Fertner, H. Kramar, and E. Meijers, "City-Ranking of European Medium-Sized Cities," *Cent. Reg. Sci. Vienna UT* 9 (2007): 1–12.

14. V. Albino, U. Berardi, and R. M. Dangelico, "Smart Cities: Definitions, Dimensions, Performance, and Initiatives," *Journal of Urban Technology* 22 (2015): 3–21.

15. O. Golubchikov, "People-Smart Sustainable Cities," Available at SSRN3757563, 2020.

16. Ú. Cárdenas-Mamani and D. Perrotti, "Understanding the Contribution of Ecosystem Services to Urban Metabolism Assessments: An Integrated Framework," *Ecological Indicators* 136 (2022): 108593.

17. S. Sofianopoulos, A. Faka, and C. Chalkias, "SDI-Enabled Smart Governance: A Review (2015–2025) of IoT, AI and Geospatial Technologies—Applications and Challenges," *Land* 14 (2025): 1399, https://doi.org/10.3390/land14071399.

18. E. Primmer and E. Furman, "How Have Measuring, Mapping and Valuation Enhanced Governance of Ecosystem Services?," *Ecosystem Services* 67 (2024): 101612, https://doi.org/10.1016/j.ecoser.2024.101612.

19. J. D. Lambert, *Numerical Methods for Ordinary Differential Systems*, vol. 146 (Wiley New York, 1991).

20. A. Edalat, A. Farjudian, M. Mohammadian, and D. Pattinson, "Domain Theoretic Second-Order Euler's Method for Solving Initial Value Problems," *Electronic Notes in Theoretical Computer Science* 352 (2020): 105–128.

21. C. Molthrop, *A Comparison of Euler and Runge-Kutta Methods* (John & Wiley, 2018).

22. K. Anoh, S. Maharjan, A. Ikpehai, Y. Zhang, and B. Adebisi, "Energy Peer-To-Peer Trading in Virtual Microgrids in Smart Grids: A

Game-Theoretic Approach," *IEEE Transactions on Smart Grid* 11, no. 2 (2019): 1264–1275.

23. W. Leontief and A. Strout, "Multiregional Input-Output Analysis," in *Structural Interdependence and Economic Development: Proceedings of an International Conference on Input-Output Techniques, Geneva, September 1961* (Palgrave Macmillan UK, 1963), 119–150.

24. W. Leontief, *Input-Output Economics* (Oxford University Press, 1986).

25. [25] S. Kerimkhulle, Z. Alimova, A. Slanbekova, N. Baizakov, G. Azieva, and M. Koishybayeva, "April. the Use Leontief Input-Output Model to Estimate the Resource and Value Added," in SIST2022–2022 International Conference on Smart Information Systems and Technologies, 2022.

26. E. Kropat, S. Meyer-Nieberg, and G. W. Weber, "Computational Networks and Systems–Homogenization of Variational Problems on Micro-Architectured Networks and Devices," *Optimization Methods and Software* 34, no. 3 (2019): 586–611.

27. G.-W. Weber, S. Z. Alparslan-Gök, and B. Et Söyler, "A new mathematical approach in environmental and life sciences: gene–environment networks and their dynamics," *Environmental Modeling & Assessment* 14, no. 2 (2009): 267–288.

28. "National Characterarea Profile. Blackmoor Vale and Vale of Wardour - Natural Capital and Key Ecosystem Services," 2020, https://publications.naturalengland.org.uk/file/5934553529057280.

29. S. Abuasad, A. Yildirim, I. Hashim, S. A. Abdul Karim, and J. Gómez-Aguilar, "Fractional Multi-Step Differential Transformed Method for Approximating a Fractional Stochastic SIS Epidemic Model With Imperfect Vaccination," *International Journal of Environmental Research and Public Health* 16 (2019): 973.

30. R. E. Mickens, "Exact Solutions to a Finite-Difference Model of a Nonlinear Reaction-Advection Equation: Implications for Numerical Analysis," *Numerical Methods for Partial Differential Equations* 5 (1989): 313–325.

31. S. Kanwal, M. K. Siddiqui, E. Bonyah, K. Sarwar, T. S. Shaikh, and N. Ahmed, "Analysis of the Epidemic Biological Model of Tuberculosis (TB) via Numerical Schemes," *Complexity* 2022 (2022): 5147951.

32. S. R.-J. Jang, "Non-Standard Finite Difference Methods and Biological Models," in *Advances in the Applications of Non-Standard Finite Difference Schemes*, ed. World Scientific (World Scientific Publishing Company, 2005), 423–457.

33. A. B. Gumel, K. C. Patidar, and R. J. Spiteri, "Asymptotically Consistent Non-standard Finite-difference Methods for Solving Mathematical Models Arising in Population Biology," in *Advances in the Applications of Non-Standard Finite Difference Schemes*, ed. World Scientific (World Scientific Publishing Company, 2005), 385–421.

34. B. Bernal, L. T. Murray, and T. R. H. Pearson, "Global Carbon Dioxide Removal Rates From Forest Landscape Restoration Activities," *Carbon Balance and Management* 13 (2018): 22, https://doi.org/10.1186/s13021-018-0110-8.

35. J. P. Schägner, L. Brander, J. Maes, M. L. Paracchini, and V. Hartje, "Mapping Recreational Visits and Values of European National Parks by Combining Statistical Modelling and Unit Value Transfer," *Journal for Nature Conservation* 31 (2016): 71–84.

36. J. P. Schägner, J. Maes, L. Brander, M. L. Paracchini, V. Hartje, and G. Dubois, "Monitoring Recreation Across European Nature Areas: A Geo-Database of Visitor Counts, a Review of Literature and a Call for a Visitor Counting Reporting Standard," *Journal of Outdoor Recreation and Tourism* 18 (2017): 44–55, https://doi.org/10.1016/j.jort.2017.02.004.

37. J. Sun, F. Mao, H. Du, et al., "Improving the Simulation Accuracy of the Net Ecosystem Productivity of Subtropical Forests in China: Sensitivity Analysis and Parameter Calibration Based on the BIOME-BGC Model," *Forests* 15 (2024): 552, https://doi.org/10.3390/f15030552.

38. S. Li, B. Waring, J. Powers, and D. Medvigy, "Tropical Dry Forest Response to Nutrient Fertilization: A Model Validation and Sensitivity Analysis," *Biogeosciences* 21 (2024): 455–471, https://doi.org/10.5194/bg-21-455-2024.

39. C. A. Famiglietti, T. L. Smallman, P. A. Levine, et al., "Optimal Model Complexity for Terrestrial Carbon Cycle Prediction," *Biogeosciences* 18 (2021): 2727–2754, https://doi.org/10.5194/bg-18-2727-2021.

40. M. Fritsch, H. Lischke, and K. M. Meyer, *Scaling Methods in Ecological Modelling, Methods in Ecology and Evaluation* (British Ecological Society, 2020).

41. K. C. Okafor and Natural Capital Team, "Woodland Natural Capital Accounts, UK," Office for National Statistics, accessed February 28, 2026, https://www.ons.gov.uk/economy/environmentalaccounts/bulletins/woodlandnaturalcapitalaccountsuk/2024.

42. W. Zhu and Y. Ding, "Integrating Decision Tools for Environmental Impact Reduction in Sustainable Urban Planning," *IEEE Access* 13 (2025): 30212–30234, https://doi.org/10.1109/ACCESS.2025.3540140.

43. "The Uk's Modern Industrial Strategy, Cp 1337," 2025.

Appendix A

The Appendix A provides further information on how the models are developed.

Steps for Determining X_{n+1}, Y_{n+1} and Z_{n+1}

Step I:

$$P_1 = h\left[\varphi X_n + \delta\gamma\left(1-\frac{X_n}{K_1}\right)\left(\frac{Y_n}{K_2}\right)^{\alpha_1} + \zeta Y_n + \rho Z_n - (\omega+\theta)X_n\right],$$

$$Q_1 = h\left[\psi Y_n + \pi\varepsilon\left(1-\frac{Y_n}{K_4}\right)\left(\frac{X_n}{K_3}\right)^{\alpha_2} + \omega X_n + \phi Z_n - (\zeta+\upsilon)Y_n\right],$$

$$R_1 = h\left[\Lambda Z_n + \eta\sigma\left(1-\frac{Z_n}{K_5}\right)\left(\frac{X_n}{K_3}\right)^{\alpha_3}\left(\frac{Y_n}{K_2}\right)^{\alpha_4} + \theta X_n + \upsilon Y_n - (\rho+\phi)Z_n\right].$$

Step II:

$$P_2 = h\left[\varphi\left(X_n+\frac{P_1}{2}\right) + \delta\gamma\left(1-\frac{\left(X_n+\frac{P_1}{2}\right)}{K_1}\right)\left(\frac{\left(Y_n+\frac{Q_1}{2}\right)}{K_2}\right)^{\alpha_1} + \zeta\left(Y_n+\frac{Q_1}{2}\right) + \rho\left(Z_n+\frac{R_1}{2}\right) - (\omega+\theta)\left(X_n+\frac{P_1}{2}\right)\right],$$

$$Q_2 = h\left[\psi\left(Y_n+\frac{Q_1}{2}\right) + \pi\varepsilon\left(1-\frac{\left(Y_n+\frac{Q_1}{2}\right)}{K_4}\right)\left(\frac{\left(X_n+\frac{P_1}{2}\right)}{K_3}\right)^{\alpha_2} + \omega\left(X_n+\frac{P_1}{2}\right) + \phi\left(Z_n+\frac{R_1}{2}\right) - (\zeta+\upsilon)\left(Y_n+\frac{Q_1}{2}\right)\right],$$

$$R_2 = h\left[\Lambda\left(Z_n+\frac{R_1}{2}\right) + \eta\sigma\left(1-\frac{\left(Z_n+\frac{R_1}{2}\right)}{K_5}\right)\left(\frac{\left(X_n+\frac{P_1}{2}\right)}{K_3}\right)^{\alpha_3} \times \left(\frac{\left(Y_n+\frac{Q_1}{2}\right)}{K_2}\right)^{\alpha_4} + \theta\left(X_n+\frac{P_1}{2}\right) + \upsilon\left(Y_n+\frac{Q_1}{2}\right) - (\rho+\phi)\left(Z_n+\frac{R_1}{2}\right)\right].$$

Step III:

$$P_3 = h\left[\varphi\left(X_n + \frac{P_2}{2}\right) + \delta\gamma\left(1 - \frac{\left(X_n + \frac{P_2}{2}\right)}{K_1}\right)\left(\frac{\left(Y_n + \frac{Q_2}{2}\right)}{K_2}\right)^{\alpha_1} + \zeta\left(Y_n + \frac{Q_2}{2}\right) + \rho\left(Z_n + \frac{R_2}{2}\right) - (\omega+\theta)\left(X_n + \frac{P_2}{2}\right)\right],$$

$$Q_3 = h\left[\psi\left(Y_n + \frac{Q_2}{2}\right) + \pi\varepsilon\left(1 - \frac{\left(Y_n + \frac{Q_2}{2}\right)}{K_4}\right)\left(\frac{\left(X_n + \frac{P_2}{2}\right)}{K_3}\right)^{\alpha_2} + \omega\left(X_n + \frac{P_2}{2}\right) + \phi\left(Z_n + \frac{R_2}{2}\right) - (\zeta+\upsilon)\left(Y_n + \frac{Q_2}{2}\right)\right],$$

$$R_3 = h\left[\Lambda\left(Z_n + \frac{R_2}{2}\right) + \eta\sigma\left(1 - \frac{\left(Z_n + \frac{R_2}{2}\right)}{K_5}\right)\left(\frac{\left(X_n + \frac{P_2}{2}\right)}{K_3}\right)^{\alpha_3}\left(\frac{\left(Y_n + \frac{Q_2}{2}\right)}{K_2}\right)^{\alpha_4} + \theta\left(X_n + \frac{P_2}{2}\right) + \upsilon\left(Y_n + \frac{Q_2}{2}\right) - (\rho+\phi)\left(Z_n + \frac{R_2}{2}\right)\right].$$

Step IV:

$$P_4 = h\left[\varphi\left(X_n + P_3\right) + \delta\gamma\left(1 - \frac{\left(X_n + P_3\right)}{K_1}\right)\left(\frac{\left(Y_n + Q_3\right)}{K_2}\right)^{\alpha_1} + \zeta\left(Y_n + Q_3\right) + \rho\left(Z_n + R_3\right) - (\omega+\theta)\left(X_n + P_3\right)\right],$$

$$Q_4 = h\left[\psi\left(Y_n + Q_3\right) + \pi\varepsilon\left(1 - \frac{\left(Y_n + Q_3\right)}{K_4}\right)\left(\frac{\left(X_n + P_3\right)}{K_3}\right)^{\alpha_2} + \omega\left(X_n + P_3\right) + \phi\left(Z_n + R_3\right) - (\zeta+\upsilon)\left(Y_n + Q_3\right)\right],$$

$$R_4 = h\left[\Lambda\left(Z_n + R_3\right) + \eta\sigma\left(1 - \frac{\left(Z_n + R_3\right)}{K_5}\right)\left(\frac{\left(X_n + P_3\right)}{K_3}\right)^{\alpha_3} \times \left(\frac{\left(Y_n + Q_3\right)}{K_2}\right)^{\alpha_4} + \theta\left(X_n + P_3\right) + \upsilon\left(Y_n + Q_3\right) - (\rho+\phi)\left(Z_n + R_3\right)\right].$$

We shall observe that the incremental in the value of P_{n+1}, Q_{n+1} and R_{n+1} is then

$$X_{n+1} = X_n + \frac{1}{6}\left[P_1 + 2P_2 + 2P_3 + P_4\right],$$

$$Y_{n+1} = Y_n + \frac{1}{6}\left[Q_1 + 2Q_2 + 2Q_3 + Q_4\right],$$

$$Z_{n+1} = Z_n + \frac{1}{6}\left[R_1 + 2R_2 + 2R_3 + R_4\right].$$

Partial Derivatives of A, B and C With Respect to X, Y and Z, Respectively

$$\frac{\partial A}{\partial X} = \frac{1}{1 + h\delta\gamma\left(\frac{1}{K_1}\right)\left(\frac{Y}{K_2}\right) + h(\omega+\theta) - h\varphi},$$

$$\frac{\partial A}{\partial Y} = \frac{\left(\frac{h\delta\gamma}{K_2} + h\zeta\right)(1 + h(\omega+\theta) - h\varphi) - \left(\frac{h\delta\gamma}{K_1K_2}\right)(X + h\rho Z)}{\left(1 + h\delta\gamma\left(\frac{1}{K_1}\right)\left(\frac{Y}{K_2}\right) + h(\omega+\theta) - h\varphi\right)^2},$$

$$\frac{\partial A}{\partial Z} = \frac{h\rho}{1 + h\delta\gamma\left(\frac{1}{K_1}\right)\left(\frac{Y}{K_2}\right) + h(\omega+\theta) - h\varphi}.$$

Similarly,

$$\frac{\partial B}{\partial X} = \frac{(1 + h(\zeta+\upsilon) - h\psi)\left(\frac{h\pi\varepsilon}{K_3} + h\omega\right) - (Y + h\phi Z)\left(\frac{h\pi\varepsilon}{K_3K_4}\right)}{\left(1 + h\pi\varepsilon\left(\frac{1}{K_4}\right)\left(\frac{X}{K_3}\right) + h(\zeta+\upsilon) - h\psi\right)^2},$$

$$\frac{\partial B}{\partial Y} = \frac{1}{1 + h\pi\varepsilon\left(\frac{1}{K_4}\right)\left(\frac{X}{K_3}\right) + h(\zeta+\upsilon) - h\psi},$$

$$\frac{\partial B}{\partial Z} = \frac{h\phi}{1 + h\pi\varepsilon\left(\frac{1}{K_4}\right)\left(\frac{X}{K_3}\right) + h(\zeta+\upsilon) - h\psi}.$$

Finally

$$\frac{\partial C}{\partial X} = \frac{(1 + h(\rho+\phi) - h\Lambda)\left(\frac{h\eta\sigma Y}{K_3K_4} + h\theta\right) - (Z + h\upsilon Y)\left(\frac{h\eta\sigma Y}{K_2K_3K_5}\right)}{\left(1 + h\eta\sigma\left(\frac{1}{K_5}\right)\left(\frac{X}{K_3}\right)\left(\frac{Y}{K_2}\right) + h(\rho+\phi) - h\Lambda\right)^2},$$

$$\frac{\partial C}{\partial Y} = \frac{(1 + h(\rho+\phi) - h\Lambda)\left(\frac{h\eta\sigma X}{K_3K_4} + h\upsilon\right) - (Z + h\theta X)\left(\frac{h\eta\sigma X}{K_2K_3K_5}\right)}{\left(1 + h\eta\sigma\left(\frac{1}{K_5}\right)\left(\frac{X}{K_3}\right)\left(\frac{Y}{K_2}\right) + h(\rho+\phi) - h\Lambda\right)^2},$$

$$\frac{\partial C}{\partial Z} = \frac{1}{1 + h\eta\sigma\left(\frac{1}{K_5}\right)\left(\frac{X}{K_3}\right)\left(\frac{Y}{K_2}\right) + h(\rho+\phi) - h\Lambda}.$$

Determining the Jacobian Matrix Elements

$$A_{11} = \frac{\partial A}{\partial X} = \frac{1}{1 + h\delta\gamma\left(\frac{1}{K_1}\right)\left(\frac{Y}{K_2}\right) + h(\omega+\theta) - h\varphi},$$

$$A_{12} = \frac{\partial A}{\partial Y} = \frac{\left(\frac{h\delta\gamma}{K_2} + h\zeta\right)(1 + h(\omega+\theta) - h\varphi) - \left(\frac{h\delta\gamma}{K_1K_2}\right)(X + h\rho Z)}{\left(1 + h\delta\gamma\left(\frac{1}{K_1}\right)\left(\frac{Y}{K_2}\right) + h(\omega+\theta) - h\varphi\right)^2},$$

$$A_{13} = \frac{\partial A}{\partial Z} = \frac{h\rho}{1 + h\delta\gamma\left(\frac{1}{K_1}\right)\left(\frac{Y}{K_2}\right) + h(\omega+\theta) - h\varphi},$$

$$B_{21} = \frac{\partial B}{\partial X} = \frac{(1 + h(\zeta+\upsilon) - h\psi)\left(\frac{h\pi\varepsilon}{K_3} + h\omega\right) - (Y + h\phi Z)\left(\frac{h\pi\varepsilon}{K_3K_4}\right)}{\left(1 + h\pi\varepsilon\left(\frac{1}{K_4}\right)\left(\frac{X}{K_3}\right) + h(\zeta+\upsilon) - h\psi\right)^2},$$

$$B_{22} = \frac{\partial B}{\partial Y} = \frac{1}{1 + h\pi\varepsilon\left(\frac{1}{K_4}\right)\left(\frac{X}{K_3}\right) + h(\zeta+\upsilon) - h\psi},$$

$$B_{23} = \frac{\partial B}{\partial Z} = \frac{h\phi}{1 + h\pi\varepsilon\left(\frac{1}{K_4}\right)\left(\frac{X}{K_3}\right) + h(\zeta+\upsilon) - h\psi},$$

$$C_{31} = \frac{\partial C}{\partial X} = \frac{(1 + h(\rho + \phi) - h\Lambda)\left(\frac{h\eta\sigma Y}{K_3K_4} + h\theta\right) - (Z + h\upsilon Y)\left(\frac{h\eta\sigma Y}{K_2K_3K_5}\right)}{\left(1 + h\eta\sigma\left(\frac{1}{K_5}\right)\left(\frac{X}{K_3}\right)\left(\frac{Y}{K_2}\right) + h(\rho + \phi) - h\Lambda\right)^2},$$

$$C_{32} = \frac{\partial C}{\partial Y} = \frac{(1 + h(\rho + \phi) - h\Lambda)\left(\frac{h\eta\sigma X}{K_3K_4} + h\upsilon\right) - (Z + h\theta X)\left(\frac{h\eta\sigma X}{K_2K_3K_5}\right)}{\left(1 + h\eta\sigma\left(\frac{1}{K_5}\right)\left(\frac{X}{K_3}\right)\left(\frac{Y}{K_2}\right) + h(\rho + \phi) - h\Lambda\right)^2},$$

$$C_{33} = \frac{\partial C}{\partial Z} = \frac{1}{1 + h\eta\sigma\left(\frac{1}{K_5}\right)\left(\frac{X}{K_3}\right)\left(\frac{Y}{K_2}\right) + h(\rho + \phi) - h\Lambda}.$$

Absolute Difference Values

From Table A1, we can find that the largest absolute value difference of the solution of $X(t)$ in interval [0,100] is 2582.34, when $t = 70$, the largest absolute value difference of the solution of $Y(t)$ in interval [0,100] is 76548.40 when $t = 40$, and the largest absolute value difference of the solution of $Z(t)$ in interval [0,100] is 87287.77 when $t = 40$. From the data, we can conclude that the absolute value differences between the two methods are large.

From Table A2, we can find that the largest absolute value difference of the solution of $X(t)$ in interval [0,100] is 23496.96 when $t = 100$, the largest absolute value difference of the solution of $Y(t)$ in interval [0,100] is 138323.99 when $t = 60$, and the largest absolute value difference of the solution of $Z(t)$ in interval [0,100] is 364523.25 when $t = 60$. From the data, we can also conclude that the absolute value differences between the two methods are large.

From Table A3, we can find that the largest absolute value difference of the solution of $X(t)$ in the interval [0,100] is 225.76 when $t = 20$, the largest absolute value difference of the solution of $Y(t)$ in the interval [0,100] is 93381.34 when $t = 10$, and the largest absolute value difference of the solution of $Z(t)$ in the interval [0,100] is 356.45 when $t = 10$. From the data, we can observe that the absolute value differences between the two methods are large.

Tables A4 and A5 presents the percentage effectiveness of biodiversity and carbon sequestration $X(t)$, recreation and tourism $Y(t)$, and water filtration $Z(t)$ under the RK4 and NSFD numerical methods. We compute the percentage effectiveness which is the relative numerical performance index (E%), computed as the ratio of the numerical accuracy (measured by error norm reduction and convergence stability) of each method to the reference solution, expressed in percentage form $\frac{\text{high value}-\text{low value}}{\text{high value}} \times 100\%$. For example, for biodiversity and carbon sequestration (X(t)) under RK4, the effectiveness was calculated as: $\frac{216205.2-99523.6}{216205.2} \times 100 = 53.97\%$. This was used to quantify how efficiently each scheme captures the system dynamics across all variables. Under the RK4 method, effectiveness levels reached 53.97% for $X(t)$, 32.44% for $Y(t)$, and 59.58% for $Z(t)$, indicating high reliability in modeling ecosystem services. The NSFD method showed slightly superior performance, with 56.13% for $X(t)$, 70.61% for $Y(t)$, and 40.29% for $Z(t)$, reflecting its strength in handling nonlinear dynamics with greater stability. Across all variables, both methods demonstrated near-optimal effectiveness, that is, 55.68% for NSFD and 48.66% for RK4, with NSFD offering marginally higher precision. These results underscore the robustness of both schemes in simulating ecological outcomes, with NSFD emerging as the more accurate technique for sustainability modeling.

For the sensitivity analysis of Equations (3a–c) using the three control parameters δ, π *and* η,we use the partial derivatives of the right-hand sides w.r.t. the controls and obtain the following:

$$\left.\begin{aligned} \frac{\partial f_1}{\partial \delta} &= \gamma\left(1 - \frac{X}{K_1}\right)\left(\frac{Y}{K_2}\right)^{\alpha_1}, \\ \frac{\partial f_2}{\partial \pi} &= \varepsilon\left(1 - \frac{Y}{K_4}\right)\left(\frac{X}{K_3}\right)^{\alpha_2}, \\ \frac{\partial f_3}{\partial \eta} &= \sigma\left(1 - \frac{Z}{K_5}\right)\left(\frac{X}{K_3}\right)^{\alpha_3}\left(\frac{Y}{K_2}\right)^{\alpha_4}. \end{aligned}\right\}$$

TABLE A1 | The solutions and differences from NSFD and RK4 methods (High).

Time (t)	X(t) NSFD	X(t) RK4	abs dif X(t)	Y(t) NSFD	Y(t) RK4	abs dif Y(t)	Z(t) NSFD	Z(t) RK4	abs dif Z(t)
100	12421.94	14045.64	1623.70	49119.22	55033.62	5914.40	24537.10	15575.23	8961.87
90	12377.80	14264.53	1886.73	24606.42	53622.13	29015.71	48190.06	15044.71	33145.35
80	12412.75	14607.08	2194.33	23713.72	53368.53	29654.81	46271.56	13980.93	32290.63
70	12570.80	14995.14	2582.34	21600.10	56831.62	35231.52	45772.51	12672.09	32599.42
60	12665.99	15120.08	2454.09	19683.27	67827.02	48143.75	52716.66	11627.57	41089.09
50	11971.31	14331.02	2359.71	22504.39	90903.42	68399.03	75954.79	12126.66	63828.13
40	9122.87	11648.69	2525.82	46320.10	122868.50	76548.40	107842.22	20554.45	87287.77
30	4517.87	6626.20	2108.33	64928.28	114685.81	49756.72	77952.98	53702.05	24250.93
20	1804.46	2624.84	820.38	27020.17	49249.07	22228.90	29465.97	33266.95	3800.98
10	799.28	992.22	192.94	7424.56	21406.60	13982.04	14155.84	8785.09	5370.75

TABLE A2 | The solutions and differences from NSFD and RK4 methods (moderate).

Time (t)	X(t) NSFD	X(t) RK4	abs dif X(t)	Y(t) NSFD	Y(t) RK4	abs dif Y(t)	Z(t) NSFD	Z(t) RK4	abs dif Z(t)
100	167263.78	190760.42	23496.69	139474.39	225811.64	86337.25	355640.72	258119.73	97520.99
90	166862.33	185312.52	18450.19	133689.47	233423.65	99734.18	360758.43	260697.57	1000060.86
80	166244.22	177745.81	11501.59	128369.08	244097.66	120728.58	396816.62	262222.18	134594.44
70	161400.68	166010.93	4610.25	139780.46	271003.03	131222.57	498616.22	264031.12	234585.10
60	140824.07	148512.03	7687.96	227656.94	365980.13	138323.99	653489.59	288966.34	364523.25
50	88172.12	108046.16	19874.04	390268.65	515755.12	125486.47	574997.95	379704.04	195293.91
40	34144.30	50325.11	16180.81	226083.60	373640.54	147556.94	248768.14	301582.67	52814.53
30	11282.76	16487.64	5204.88	58136.20	143911.19	85774.99	83603.98	111000.68	27396.70
20	3661.30	4988.55	1327.25	24519.78	48269.82	23750.04	28502.0.85	32775.34	4252.49
10	1158.80	1397.31	238.51	6971.12	21280.19	14509.07	1487.06	8320.05	6832.99

TABLE A3 | The solutions and differences from NSFD and RK4 methods (low).

Time (t)	X(t) NSFD	X(t) RK4	abs dif X(t)	Y(t) NSFD	Y(t) RK4	abs dif Y(t)	Z(t) NSFD	Z(t) RK4	abs dif Z(t)
100	40.48	116.84	76.36	92.46	562.74	470.28	13.81	75.52	61.71
90	56.24	137.60	81.36	120.07	595.38	475.31	17.98	80.37	62.39
80	79.30	167.62	88.32	156.37	636.34	479.97	23.52	86.73	63.19
70	112.74	213.03	100.29.	204.79	693.73	488.94	31.06	96.20	65.14
60	163.26	280.79	117.53	272.59	781.04	516.45	42.44	111.88	69.44
50	237.25	380.78	143.53	377.19	931.57	554.38	62.07	141.96	79.89
40	343.05	520.08	177.03	566.52	1225.19	658.67	104.14	207.94	103.80
30	489.12	702.34	213.22	992.26	1928.00	935.74	213.34	378.74	165.40
20	644.10	869.86	225.76	226.87	3930.05	3703.18	525.23	820.57	295.34
10	645.92	782.35	136.43	6705.25	10086.59	3381.34	1199.74	1556.19	356.45

TABLE A4 | Percentage effectiveness in biodiversity and carbon sequestration that is, (Greenhouse gas regulation) $X(t)$, recreation and tourism $Y(t)$, and water filtration $Z(t)$ under RK4 and NSFD methods.

X(t) RK4 low	X(t) RK4 high	%Effectiveness X(t)	Y(t) RK4 low	Y(t) RK4 high	% Effectiveness Y(t)	Z(t) RK4 low	Z(t) RK4 high	%Effectiveness Z(t)
99523.6	216205.2	53.97	126233.7	186852.9	32.44	114518.3	283297.5	59.58
X(t) NSFD low	**X(t) NSFD high**	**% Effectiveness X(t)**	**Y(t) NSFD low**	**Y(t) NSFD high**	**%Effectiveness Y(t)**	**Z(t) NSFD low**	**Z(t) NSFD high**	**% Effectiveness Z(t)**
74694.5	170258.4	56.13	104857.2	356726.3	70.61	83185.7	139312.2	40.29

TABLE A5 | Normalized instantaneous sensitivity indices at $X(t), Y(t)$, and $Z(t)$with respect to control parameters δ, π and η.

t	Method	X	Y	Z	S_{δ}^{X}	S_{π}^{Y}	S_{η}^{Z}
100	NSFD	12421.94	49119.22	24537.10	−0.001243	−0.000006	−0.000107
100	RK4	14045.64	55033.62	15575.23	−0.001395	−0.000005	−0.001702
90	NSFD	12377.80	24606.42	48190.06	−0.000623	−0.000044	−0.001434
90	RK4	14264.53	53622.13	15044.71	−0.001359	−0.000005	−0.002583
80	NSFD	12412.75	23713.72	46271.56	−0.000600	−0.000047	−0.001333
80	RK4	14607.08	53368.53	13980.93	−0.001353	−0.000005	−0.002778
70	NSFD	12570.80	21600.10	45772.51	−0.000547	−0.000051	−0.001176
70	RK4	14995.14	56831.62	12672.09	−0.001441	−0.000004	−0.003862
60	NSFD	12665.99	19683.27	52716.66	−0.000498	−0.000057	−0.000896
60	RK4	15120.08	67827.02	11627.57	−0.001720	−0.000003	−0.004880
50	NSFD	11971.31	22504.39	75954.79	−0.000569	−0.000036	−0.000326
50	RK4	14331.02	90903.42	12126.66	−0.002304	−0.000003	−0.003409
40	NSFD	9122.87	46320.10	107842.22	−0.001168	−0.000011	−0.000228
40	RK4	11648.69	122868.50	20554.45	−0.003108	−0.000005	−0.005073
30	NSFD	4517.87	64928.28	77952.98	−0.001613	−0.000010	−0.000373
30	RK4	6626.20	114685.81	53702.05	−0.002083	−0.000006	−0.002281
20	NSFD	1804.46	27020.17	29465.97	−0.003542	−0.000101	−0.000177
20	RK4	2624.84	49249.07	33266.95	−0.002412	−0.000056	−0.000157
10	NSFD	799.28	7424.56	14155.84	−0.007655	−0.000277	−0.000185
10	RK4	992.22	21406.60	8785.09	−0.004579	−0.000013	−0.002008

We then formed normalized instantaneous sensitivity indices at the state $X(t), Y(t)$, and $Z(t)$by

$$S_{\varkappa}^{(\rho)} = \frac{\varkappa}{\rho} \frac{\partial f_i}{\partial \varkappa} |_{(\mathrm{X,Y,Z})}, \quad where\ \varkappa = \delta, \pi, \eta.$$

The sensitivities vary substantially over time and differ between NSFD and RK4 because the state values X, Y, Z(which appear nonlinearly in the partial derivatives) are different for the two schemes. $S_{\delta}^{(X)}$is generally small and negative here (because $1 - \frac{X}{K_1}$becomes negative when $X > K_1$, making $\frac{\partial f_1}{\partial \delta}$ negative), indicating that at many time points increasing δ would *reduce* the instantaneous growth of X (saturation). $S_{\pi}^{(Y)}$is tiny (close to zero) in many rows because $\frac{\pi}{Y}$scales the partial and Y is large. In some NSFD rows where Y is smaller, magnitude increases. $S_{\eta}^{(Z)}$varies and is often larger in magnitude for RK4 than NSFD at matching times due to differences in X, Y, Z—this helps explain why RK4 showed stronger "sensitivity" qualitatively.

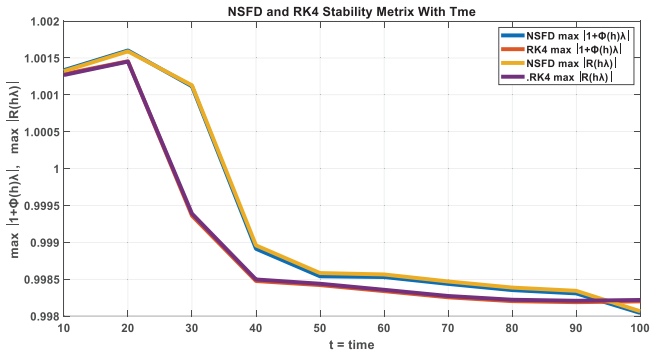

FIGURE A1 | Numerical simulation of the stability analysis of the RK4 and NSFD methods.

The stability analysis of the RK4 and NSFD methods under the high parameter set (Figure A1) shows that both methods remain below the unity stability threshold for most of the simulation, confirming numerical stability. At the beginning, both slightly exceed the threshold (≈1.001–1.002), indicating mild numerical amplification but not instability. This deviation reflects the sensitivity of the Jacobian eigenvalues under high parameter influence. The NSFD method shows smoother damping and better control than RK4. Overall, both methods are stable for $h = 0.02$, with NSFD exhibiting superior robustness.

Local Error Estimate for High and Low Scenario

Using RK4 as the reference, we have the pointwise error as $NSFD - RK4$. Then, the internal step is $h = 0.02$ and the sampling interval between reported points is $\Delta T_{sample} = 10$. Therefore, we have the number of internal steps between samples as

$$N_{steps} = \frac{\Delta T_{sample}}{h} = 500.$$

The per-step local error estimate is computed as the average error accumulated per internal step over the sample interval:

$$\hat{\tau}_q = \frac{\mathcal{Q}_{NSFD}(t) - \mathcal{Q}_{RK4}(t)}{N_{steps}} = \frac{err_q(t)}{500}.$$

The analysis of the low parameter scenario in Table A6 reveals that both the RK4 and NSFD schemes maintain numerical stability throughout the simulation period, although their local error magnitudes differ slightly. The error estimates for the state variables $X(t)$, $Y(t)$, and $Z(t)$ remain relatively small, with gradual changes over time. The per-step local errors (τ_X, τ_Y, τ_Z) are all within manageable ranges, suggesting that the system's response is smooth and well-conditioned under low parameter influence. Specifically, $X(t)$ and $Z(t)$ exhibit slower error growth, while $Y(t)$ shows slightly higher deviations, reflecting its stronger sensitivity to parameter variations and interaction effects. As time progresses, a mild increase in numerical deviation is noticed due to the accumulation of local truncation errors inherent in both schemes. However, the NSFD method produces more stable and closely bound error patterns compared to RK4. This is evident from its consistent underestimation trend and smaller per-step deviations. This outcome highlights the effectiveness of the NSFD scheme in preserving boundedness and stability even with longer time integration, confirming its advantage for systems characterized by slow nonlinear interactions or weak feedback dynamics.

Conversely, the high parameter scenario in Table A7 demonstrates a more complex and amplified error structure, mainly due to the system's stronger nonlinear coupling and parameter intensities. In this regime, the magnitudes of *errX*, *errY*, and *errZ*rise sharply, showing significant fluctuations that indicate higher stiffness and sensitivity of the underlying model. The local error per step (τ) increases substantially, reflecting the heightened response of the model to parameter perturbations and time-step propagation. While RK4 captures the rapid variations efficiently at early stages, it tends to amplify local oscillations as the simulation progresses, particularly for $Y(t)$ and $Z(t)$. In contrast, the NSFD scheme continues to maintain numerical damping, reducing excessive oscillations and containing error escalation near equilibrium points. This stability advantage underscores NSFD's ability to handle stiff or highly nonlinear systems without losing consistency. Overall, comparing both scenarios confirms that the NSFD method demonstrates superior error control, asymptotic stability, and robustness against parameter-induced perturbations, making it a more reliable numerical tool for simulating highly interactive and nonlinear dynamical systems.

TABLE A6 | Per–sample pointwise error and per-step τ for low scenario.

Time	err_X	τ_X (per step)	err_Y	τ_Y (per step)	err_Z	τ_Z (per step)
100	−76.36	−0.15272	−470.28	−0.94056	−61.71	−0.12342
90	−81.36	−0.16272	−475.31	−0.95062	−62.39	−0.12478
80	−88.32	−0.17664	−479.97	−0.95994	−63.19	−0.12638
70	−100.29	−0.20058	−488.94	−0.97788	−65.14	−0.13028
60	−117.53	−0.23506	−508.45	−1.01690	−69.44	−0.13888
50	−143.53	−0.28706	−554.38	−1.10876	−79.89	−0.15978
40	−177.03	−0.35406	−658.67	−1.31734	−103.80	−0.20760
30	−213.22	−0.42644	−935.74	−1.87148	−165.40	−0.33080
20	−225.76	−0.45152	−3703.18	−7.40636	−295.34	−0.59068
10	−136.43	−0.27286	−3381.34	−6.76268	−356.45	−0.71290

TABLE A7 | Per–sample pointwise error and per-step τ for high scenario.

Time	err_X	τ_X (per step)	err_Y	τ_Y (per step)	err_Z	τ_Z (per step)
100	−1623.70	−3.24740	−5914.40	−11.82880	8961.87	17.92374
90	−1886.73	−3.77346	−29015.71	−58.03142	33145.35	66.29070
80	−2194.33	−4.38866	−29654.81	−59.30962	32290.63	64.58126
70	−2424.34	−4.84868	−35231.52	−70.46304	33100.42	66.20084
60	−2454.09	−4.90818	−48143.75	−96.28750	41089.09	82.17818
50	−2359.71	−4.71942	−68399.03	−136.79806	63828.13	127.65626
40	−2525.82	−5.05164	−76548.40	−153.09680	87287.77	174.57554
30	−2108.33	−4.21666	−49756.72	−99.51344	24250.93	48.50186
20	−820.38	−1.64076	−22228.90	−44.45780	−3800.98	−7.60196
10	−192.94	−0.38588	−13982.04	−27.96408	5370.75	10.74150